JOURNAL OF GEOPHYSICAL RESEARCH, VOL. 113, E05008, doi:10.1029/2007JE002946, 2008

Click Here for Full Article

Hydrodynamic planetary thermosphere model: 1. Response of the Earth's thermosphere to extreme solar EUV conditions and the significance of adiabatic cooling

Feng Tian,[1] James F. Kasting,[2] Han-Li Liu,[1] and Raymond G. Roble[1]

Received 29 May 2007; revised 24 October 2007; accepted 22 February 2008; published 31 May 2008.

[1] It has been suggested that the exobase temperature of early terrestrial planetary atmosphere could have reached over 10,000 K. Although such high exobase temperatures should have caused the major gases at the exobase to experience fast Jeans escape, and the entire thermosphere should have experienced hydrodynamic flow, hydrostatic equilibrium was assumed to be valid in this earlier model. In this paper we develop a multicomponent hydrodynamic thermosphere model to self-consistently study the Earth's thermosphere under extreme solar EUV conditions. The model is validated against observations and other models for the present Earth's thermosphere. Simulations show that if forced in hydrostatic equilibrium and maintaining the current composition, the Earth's thermosphere could experience a fast transition to an atmospheric blowoff state when exposed to solar EUV radiation stronger than certain critical flux. When hydrodynamic flow and its associated adiabatic cooling are included, atmospheric blowoff is prevented and Earth's exobase temperature decreases with increasing solar EUV beyond the critical solar EUV flux. Simulations show that the transition of the thermosphere from the hydrostatic equilibrium regime to the hydrodynamic regime occurs when the exobase temperature reaches 7000 to 8000 K if atomic O and N dominate the upper thermosphere. The fast variations of the bulk motion velocities under different exobase temperatures suggest that the adiabatic cooling effect could have kept the exobase temperature lower than ~1000 K if light gases such as atomic hydrogen were the dominant species in the Earth's thermosphere. We propose that hydrodynamic flow and associated adiabatic cooling should exist in the thermospheres of a broad range of early and/or close-in terrestrial type planets and that the adiabatic cooling effect must be included in the energy balance in order to correctly estimate their thermospheric structures and their evolutionary paths.

Citation: Tian, F., J. F. Kasting, H.-L. Liu, and R. G. Roble (2008), Hydrodynamic planetary thermosphere model: 1. Response of the Earth's thermosphere to extreme solar EUV conditions and the significance of adiabatic cooling, *J. Geophys. Res.*, *113*, E05008, doi:10.1029/2007JE002946.

1. Introduction

[2] Studies of atmospheric escape are important for determining the evolutionary paths of planetary atmospheres. On the basis of their source of energy, escape mechanisms can be divided into two categories: thermal escape and nonthermal escape. In thermal escape, particles at the exobase are assumed to have an approximately Maxwellian velocity distribution that is determined by the exobase temperature, and those with outgoing velocities exceeding the escape velocity of the planet can escape [*Jeans*, 1925; *Walker*, 1977]. Thermal escape rate is controlled by the Jeans escape parameter, $\lambda_c = GMm/kT_{exo}r_{exo}$, which represents the ratio of the gravitational energy to the mean thermal energy of the particle, along with the number density of the escaping gas at the exobase level. An extreme case of thermal escape is atmospheric "blowoff," which occurs when the mean thermal energy of the major gases at the exobase level (where the mean free path of the gas particles is comparable to the scale height of the atmosphere) exceeds their gravitational potential energy (equivalent to $\lambda_c < 1.5$). In the blowoff state the loss of gas can be "almost arbitrarily high and indiscriminate as to species" [*Öpik*, 1963]. In this definition, atmospheric blowoff is essentially an uncontrolled process in the sense that the loss of gas (at an arbitrarily high rate) does not affect the exobase temperature. Realistically, gases should escape planetary atmospheres in a more controlled manner (limited by energy), but still faster than predicted by the Jeans' formula, because the pressure force contributes to the escape process (See further discussion below). All of the

[1] High Altitude Observatory, National Center for Atmospheric Research, Boulder, Colorado, USA.
[2] Department of Geosciences, Pennsylvania State University, University Park, Pennsylvania, USA.

Copyright 2008 by the American Geophysical Union.
0148-0227/08/2007JE002946$09.00

above escape processes are thermal. By contrast, in nonthermal escape processes, such as H/H^+ charge exchange, the escaping atoms acquire energy from nonthermal sources, in this case hot H^+ ions. The known nonthermal escape processes are summarized by *Chamberlain and Hunten* [1987].

[3] We note parenthetically that a different definition of atmospheric blowoff is given by *Chamberlain and Hunten* [1987]. They define blowoff as a condition in which the escaping light constituents are able to drag heavier constituents along with them. Blowoff, by this definition, may or may not be indiscriminate with respect to heavy species, depending on the magnitude of the light gas escape flux. We suggest that this condition should be part of regime II of planetary thermospheres defined next. In the rest of this paper, we use Öpik's definition of atmospheric blowoff.

[4] The above classification of escape mechanisms concerns only the region near and above the exobase. To understand how the underlying planetary atmosphere responds to different escape scenarios requires a thermosphere model that includes both energetics and dynamics. We propose that planetary thermospheres can be classified into two regimes: regime I is the hydrostatic equilibrium regime, in which the bulk atmosphere below the exobase can be considered as static; and regime II is the hydrodynamic flow regime, in which the major gases in the thermosphere can escape efficiently as a result of large energy input and/or a weak planetary gravitational field. The hydrodynamic flow regime is not to be considered equivalent to the atmospheric blowoff state, as suggested in some recent literature. As we will show later, a planetary atmosphere can be in the hydrodynamic flow regime without satisfying the blowoff criteria ($\lambda_c < 1.5$); indeed, the proper treatment of the hydrodynamic flow *prevents* the occurrence of atmospheric blowoff. The upper atmospheres of hydrogen-rich and water-rich early terrestrial planets [e.g., *Watson et al.*, 1981; *Kasting and Pollack*, 1983; *Chassefière*, 1996; *Tian et al.*, 2005b], those of close-in extrasolar planets [e.g., *Lammer et al.*, 2003; *Yelle*, 2004; *Tian et al.*, 2005a; *García-Muñoz*, 2007], and that of Pluto [*Krasnopolsky*, 1999; *Tian and Toon*, 2005; *Strobel*, 2008] are in the hydrodynamic flow regime. Recently, it is suggested that Titan's upper atmosphere is also in this regime [*Strobel*, 2007].

[5] Physically, when a hydrodynamic flow reaches the exobase, it must be matched by the combined escape flux caused by thermal and nonthermal processes. Because the escape flux depends on parameters (density, temperature, etc.) which are in turn controlled by the hydrodynamic flow, obtaining a self-consistent solution for the hydrodynamic flow is complicated. However, if the bulk motion velocity at the exobase exceeds the escape velocity of the planet, escape can be accomplished by the hydrodynamic flow itself and the problem is simpler. It is important to realize that even if the bulk motion velocity at the exobase level is smaller than the escape velocity, a hydrodynamic flow model may still be required in order to correctly characterize the thermospheric structure. Because of the adiabatic cooling effect of the hydrodynamic flow, the atmospheric temperature can be reduced significantly if the bulk motion velocity is substantially high, thereby preventing the occurrence of atmospheric blowoff.

[6] Hydrodynamic flow models themselves can be subdivided into two different types: subsonic and transonic. Which type of flow regime applies depends on the density of the escaping gas and the conditions at the upper boundary. In the simplest case, expansion of a dense (and, hence, collisional) fluid into a vacuum, the flow should be transonic. This solution, and no other, satisfies the condition that the mass of the atmosphere is finite if one integrates out to infinity. The solar wind is an example of such a transonic flow [*Parker*, 1963]. Although the wind itself is tenuous, it remains effectively collisional because it is fully ionized and the particles can exchange momentum through their interaction with the embedded magnetic field. The solar wind does not expand into a vacuum, of course; rather, it creates a shock front at the heliopause where it encounters the local interstellar medium. However, because the flow is already supersonic at this distance, the presence of this shock front has no effect on the flow velocities inside it.

[7] Planetary winds are more complex in the sense that they are only partially ionized, and so the escaping particles are less interconnected by long-range, electromagnetic forces. Such a flow becomes collisionless at some point, and the fluid dynamic approximation is no longer valid. If this point (the exobase) is reached beyond the critical point where the flow becomes supersonic, then the transonic solution should still be valid. But there are other possibilities as well. The flow may become collisionless before it becomes supersonic, so that the entire hydrodynamic flow regime is subsonic. Some models of this type, including the one described in this paper, apply Jeans escape effusion velocity at the upper boundary [*Chassefière*, 1996; *Yelle*, 2004]. This approach may underestimate the actual escape rate because it ignores nonthermal escape processes above the exobase. Planetary winds are also expanding into an anisotropic interplanetary medium defined by the solar wind. The interaction between the solar wind and the planet's ionosphere or magnetosphere creates a bow shock that is located at different distances depending on the strength of the planet's magnetic field and the plasma in the planet's magnetosphere. Even a dense planetary wind escaping in the sunward direction could be constrained to remain subsonic as a consequence of solar wind backpressure or, more likely, may be redirected into the antisolar hemisphere. Thus any 1-D approximation to this process is just that, an approximation. That said, much can be learned from 1-D hydrodynamic flow models, even if multidimensional models are eventually called for.

[8] The status of the current hydrodynamic modeling efforts is not satisfactory. Most hydrodynamic models for early terrestrial planetary atmospheres [e.g., *Watson et al.*, 1981; *Kasting and Pollack*, 1983; *Chassefière*, 1996; *Tian et al.*, 2005b] depend on parameterized heating efficiencies due to their lack of detailed treatments of radiative transfer. Earth thermosphere models [*Roble et al.*, 1987; *Roble*, 1995; *Smithtro and Sojka*, 2005a, 2005b], on the other hand, compute heating efficiencies self-consistently but are based on the assumption of hydrostatic equilibrium. This assumption is justifiable today, but is of questionable validity when it is extrapolated to the study of the long-term evolution of planetary atmospheres.

[9] It has been suggested that the young Sun emitted stronger EUV radiation: approximately 3, 6, and 10 times

Table 1. Boundary Conditions Corresponding to 18 Short-Lived Species[a]

	Long-Lived Species													
	O	O_2	N_2	H_e	H	H_2	CO_2	CO	N(4S)	NO	H_2O	O^+	N^+	H^+
Upper boundary condition	0	1	1	0	0	0	1	1	0	1	1	0	0	0

[a]Short-lived species are O_3, HO_2, OH, H_2^+, H_3^+, $O^+(^2P)$, $O^+(^2D)$, N_2^+, CO^+, CO_2^+, O_2^+, NO^+, OH^+, $N(^2D)$, $O(^1D)$, H_2O_2, $O_2(^1\Sigma_g)$, $O_2(^1\Delta_g)$. Conditions are 0, effusion velocity, set equal to the corresponding species' Jeans escape velocity at the exobase level; and 1, zero flux. The lower boundary condition has a fixed mixing ratio.

that of today at ~3, 3.5, and 3.8 Ga ago, respectively [*Ribas et al.*, 2005]. A few hundred million years after its formation, the Sun's EUV radiation level could have been 100 times that of today (100 times present EUV). Recently, a hydrostatic equilibrium model [*Kulikov et al.*, 2007] has been applied to the early terrestrial planetary thermospheres under a wide range of solar EUV radiation levels (1–100 times present EUV). For early Earth with the same composition as that of today, the model predicted a thermospheric temperature of ~10,000 K for ~12 times present EUV condition [*Kulikov et al.*, 2007]. The extremely high thermospheric temperatures of *Kulikov et al.* [2007] suggest that the thermosphere cannot be considered hydrostatic in extreme solar EUV conditions because atomic oxygen (the dominant gas in the upper thermosphere of the present Earth) should be escaping at a significant rate.

[10] Although some of the more recent hydrodynamic models [*Krasnopolsky*, 1999; *Yelle*, 2004] included detailed radiative transfer treatments, the chemical schemes in these models are designed for the atmospheres of either giant planets or Pluto, which limits their applicability to the terrestrial planets. The motivation of this work is to develop a general thermosphere model which can be applied to various types of planetary atmospheres while accounting for potentially important hydrodynamic flow and the associated adiabatic cooling. In this paper we describe a 1-D, multicomponent hydrodynamic thermospheric model, and we use it to explore the response of the Earth's thermosphere under extreme solar EUV radiation conditions. Application to early Earth-type atmospheres will be given in a future paper. The details of the model are described in section 2. In section 3 the model is validated against the observations (NRL mass spectrometer incoherent scatter radar extended model [*Hedin*, 1991], hereafter MSIS-00) and existing theoretical models [*Roble et al.*, 1987; *Roble*, 1995; *Smithtro and Sojka*, 2005a, 2005b]. The responses of the Earth's thermosphere to extreme solar EUV radiations and the significance of the adiabatic cooling effect are the topics of section 4. The discussion and conclusions are given in sections 5 and 6.

2. Model Description

[11] The model treats the whole thermosphere as a single fluid with a varying mean molecular mass. Similar to the treatment by *Kasting and Pollack* [1983], the model iteratively solves the momentum and energy equations for this moving atmosphere. In order to treat the energy deposition self-consistently and to avoid having to parameterize the overall heating efficiency, the model includes both neutral and ion species. Time-independent diffusion equations are solved for 14 long-lived species, and chemical equilibrium is applied to 18 short-lived species. These species and their corresponding boundary conditions are listed in Table 1. Quasi-charge neutrality is assumed in the model. The model includes 154 chemical reactions, collected from thermospheric models of the present Earth [*Roble*, 1995; *Smithtro and Sojka*, 2005a], Venus/Mars [*Nagy et al.*, 1983; *Barth et al.*, 1992; *Fox and Delgarno*, 1979], and extrasolar planets [*Yelle*, 2004]. The list of reactions, reaction rates, energy released/absorbed, and the references is given in Table 2. The lower boundary of the model is at ~95 km and the top boundary is the exobase, whose position is determined iteratively throughout the calculation by comparing the mean free path and the scale height of the background gas. When the upper boundary is found to be below the exobase, the upper boundary is expanded by 1/4 of a scale height at each time step until the exobase is matched. Note that because the gravity decreases with increasing altitude, the upper boundary altitude does not necessarily reside on a constant pressure surface. The model grid points are spaced unequally in altitude so that each scale height includes at least 4 grid points. More grid points are used under stronger solar EUV conditions.

[12] The 1-D hydrodynamic, thermospheric model solves the continuity, momentum, and energy equations in a moving atmosphere. We start from the 1-D, time-dependent, nonviscous hydrodynamic equation set of *Tian et al.* [2005a]:

$$\begin{aligned} \frac{\partial(\rho r^2)}{\partial t} + \frac{\partial(\rho u r^2)}{\partial r} &= 0, \\ \frac{\partial(\rho u r^2)}{\partial t} + \frac{\partial(\rho u^2 r^2 + p r^2)}{\partial r} &= -\rho G M + 2pr, \\ \frac{\partial(E r^2)}{\partial t} + \frac{\partial[(E+p)u r^2]}{\partial r} &= -\rho u G M + q r^2 + \frac{\partial}{\partial r}\left(\kappa r^2 \frac{\partial T}{\partial r}\right), \end{aligned} \tag{1}$$

with

$$E = \rho\left(u^2/2 + e\right), e = \frac{p}{\rho(\gamma - 1)}, p = \rho R T.$$

Here ρ is gas density, r is distance from the planet center, u is bulk motion velocity of background gas, p is pressure, G is universal gravitational constant, M is mass of the planet, E is total energy density (which is the sum of the kinetic energy density and the internal energy density of the gas flow), κ is thermal conductivity, T is temperature, γ is adiabatic constant, R is molar gas constant, and q is volume heating rate.

[13] Because we are interested in the steady state solution, the continuity and the momentum equations are rewritten

Table 2. Chemical Reactions, Reaction Rates, Energy Associated, and the References[a]

No.	Reaction	Reaction Rate, $cm^3\ s^{-1}$	Reference
1	$N(^4S) + O_2 = NO + O + 1.40$ eV	4.4E-12 exp(−3220/T)	A
2	$N(^4S) + NO = N_2 + O + 2.68$ eV	1.6E-10 exp(−460/T)	B
3	$N(^2D) + O = N(^4S) + O + 2.38$ eV	6.90E-13	C
4	$N(^2D) + O_2 = NO + O(^1D) + 1.84$ eV	6.2E-12 × v(T/300) × 0.1	Estimated
5	$N(^2D) + O_2 = NO + O + 3.76$ eV	6.2E-12 × v(T/300) × 0.9	Estimated
6	$N(^2D) + NO = N_2 + O + 5.63$ eV	7E-11	B
7	$N(^2D) = N(^4S) + h\nu$	1.06E-05	B
8	$O(^1D) + N_2 = O + N_2 + 1.96$ eV	1.8E-11 exp(107/T)	B
9	$O(^1D) = O + h\nu$	8.33E-03	D
10	$O(^1D) + H_2O = OH + OH + 1.23$ eV	2.20E-10	B
11	$O + O + M = O_2 + M + 5.10$ eV	9.59E-34exp(480/T) [M]	B
12	$O + O_2 + M = O3 + M + 1.10$ eV	6E-34 (300./T) × 2.3 [M]	E
13	$O + O3 = O_2 + O_2 + 4.06$ eV	8E-12 exp(−2060/T)	B
14	$CO + O + M = CO_2 + M + 5.51$ eV	6.6E-33 exp(−1103/T) [M]	B
15	$H_2 + O(^1D) = H + OH + 1.88$ eV	1E-10	B
16	$H_2 + O = H + OH + 0.08$ eV	1.6E-11 exp(−4570/T)	B
17	$H_2 + M = H + H + M + -4.52$ eV	1.5E-9 exp(−4.8E4/T)	F
18	$H + O_2 = O + OH + -0.72$ eV	3.7E-10 exp(−8450/T)	G
19	$H + O3 = OH + O_2 + 3.34$ eV	1.4E-10 exp(−470/T)	B
20	$H + H + M = H_2 + M + 4.52$ eV	5.7E-32 $(300/T)^{1.6}$ [M]	B
21	$H + H_2O = H_2 + OH + -0.65$ eV	1.5E-10 exp(−10,250/T)	G
22	$OH + N(^4S) = NO + H + 2.10$ eV	5E-11	B
23	$OH + O = H + O_2 + 0.72$ eV	2E-11 exp(117/T)	B
24	$OH + CO = CO_2 + H + 1.07$ eV	1.5E-13 (1. + 0.6 PATM)	E
25	$OH + H_2 = H_2O + H + 0.65$ eV	7.7E-12 exp(−2100/T)	B
26	$OH + OH = H_2O + O + 0.73$ eV	4.2E-12 exp(−240/T)	B
27	$OH + H + M = H_2O + M + 5.17$ eV	6.1E-26 T^{-2} [M]	G
28	$OH + H = H_2 + O + 0.08$ eV	1.4E-14 T exp(−3500/T)	G
29	$N_2^+ + O_2 = O_2^+ + N_2 + 3.52$ eV	5E-11 (300/Ti)	D
30	$N_2^+ + O = NO^+ + N(^2D) + 0.70$ eV	K30	B
31	$N_2^+ + O = O^+ + N_2 + 1.96$ eV	K31	D
32	$N_2^+ + NO = NO^+ + N_2 + 6.25$ eV	4.1E-10	H
33	$N_2^+ + CO_2 = CO_2^+ + N_2 + 1.81$ eV	8E-10	H
34	$N_2^+ + CO = CO^+ + N_2 + 1.57$ eV	7.40E-11	I
35	$N^+ + O_2 = O^+ + NO + 1.28$ eV	4.60E-10	H
36	$N^+ + O_2 = O_2^+ + N(^2D) + 0.10$ eV	3.07E-10 × 0.66	C
37	$N^+ + O_2 = O_2^+ + N(^4S) + 2.49$ eV	3.07E-10 × 0.33	C
38	$N^+ + O_2 = NO^+ + O + 6.70$ eV	2.32E-10	D
39	$N^+ + O = O^+ + N(^4S) + 0.98$ eV	1E-12	B
40	$N^+ + NO = NO^+ + N(^4S) + 5.29$ eV	9E-10	J
41	$N^+ + CO_2 = CO_2^+ + N(^4S) + 0.78$ eV	9.2E-10	H
42	$N^+ + CO_2 = CO^+ + NO + 1.57$ eV	2E-10	H
43	$N^+ + CO = CO^+ + N(^4S) + 0.54$ eV	4E-10	J
44	$N^+ + H = H^+ + N(^4S) + 0.90$ eV	3.6E-12	C
45	$O_2^+ + N_2 = NO^+ + NO + 0.93$ eV	5E-16	D
46	$O_2^+ + N(^4S) = NO^+ + O + 4.21$ eV	1.5E-10	H
47	$O_2^+ + NO = NO^+ + O_2 + 2.81$ eV	4.4E-10	B
48	$O^+ + NO = NO^+ + O + 4.36$ eV	8E-13	H
49	$O^+ + CO_2 = O_2^+ + CO + 1.20$ eV	1.1E-09	H
50	$O^+ + H_2 = OH^+ + H + 0.36$ eV	2E-09	B
51	$O^+ + H = H^+ + O + 0.02$ eV	6E-10	B
52	$O^+ + N_2 = NO^+ + N(^4S) + 1.09$ eV	K52	B
53	$O^+ + O_2 = O_2^+ + O + 1.56$ eV	K53	B
54	$O^+ + N(^2D) = N^+ + O + 1.45$ eV	1.3E-10	B
55	$O^+(^2P) + N_2 = N_2^+ + O + 3.02$ eV	4.8E-10	C
56	$O^+(^2P) + N_2 = N^+ + NO + 0.70$ eV	1E-10	C
57	$O^+(^2P) + O = O^+ + O + 5.20$ eV	5.2E-11	C
58	$O^+(^2P) = O^+ + h\nu$	0.047	C
59	$O^+(^2P) = O^+(^2D) + h\nu$	0.171	C
60	$O^+(^2D) + N_2 = O^+ + N_2 + 3.31$ eV	8E-10	C
61	$O^+(^2D) + N_2 = N_2^+ + O + 1.33$ eV	1E-10	C
62	$O^+(^2D) + O = O^+ + O + 3.31$ eV	1E-11	C
63	$O^+(^2D) + O_2 = O_2^+ + O + 4.87$ eV	7E-10	C
64	$O^+(^2D) = O^+ + h\nu$	7.7E-05	C
65	$H_2^+ + O = OH^+ + H + 2.17$ eV	1.5E-09	K
66	$H_2^+ + H_2 = H_3^+ + H + 1.70$ eV	2E-09	F
67	$H_2^+ + H = H^+ + H_2 + 1.83$ eV	6.4E-10	F
68	$H^+ + O = O^+ + H + -0.02$ eV	K68	B
69	$H^+ + NO = NO^+ + H + 4.34$ eV	1.9E-09	J
70	$H^+ + H_2 = H_2^+ + H + -1.83$ eV	1E-9 exp(−2.19E4/T)	F
71	$H_3^+ + H = H_2^+ + H_2 + -1.70$ eV	2E-09	Estimated in F
72	$CO_2^+ + O = O_2^+ + CO + 1.33$ eV	1.6E-10	I
73	$CO_2^+ + O = O^+ + CO_2 + 0.13$ eV	1E-10	I

Table 2. (continued)

No.	Reaction	Reaction Rate, $cm^3\ s^{-1}$	Reference
74	$CO_2^+ + NO = NO^+ + CO_2 + 4.51$ eV	1.2E-10	I
75	$CO_2^+ + H = H^+ + CO_2 + 0.17$ eV	1E-10	J
76	$CO^+ + O = O^+ + CO + 0.39$ eV	1.4E-10	J
77	$CO^+ + NO = NO^+ + CO + 4.75$ eV	3.3E-10	J
78	$CO^+ + CO_2 = CO_2^+ + CO + 0.24$ eV	1.1E-09	I
79	$N_2^+ + e = N(^4S) + N(^4S) + 5.82$ eV	2.2E-7 $(300/Te)^{0.39}$ 0.1	D
80	$N_2^+ + e = N(^4S) + N(^4D) + 3.44$ eV	2.2E-7 $(300/Te)^{0.39}$ 0.9	D
81	$N^+ + e = N(^4S) + h\nu$	3.6e-12 $(250/Te)^{0.7}$	H
82	$O_2^+ + e = O + O + 6.99$ eV	k82	D
83	$O_2^+ + e = O + O(^1D) + 5.02$ eV	k83	D
84	$O_2^+ + e = O(^1D) + O(^1D) + 3.06$ eV	k84	D
85	$O^+ + e = O + h\nu$	3.7e-12 $(250/Te)^{0.7}$	H
86	$NO^+ + e = N(^4S) + O + 2.75$ eV	4.2E-7 $(300/Te)^{0.85}$ 0.2	B
87	$NO^+ + e = N(^2D) + O + 0.38$ eV	4.2E-7 $(300/Te)^{0.85}$ 0.8	B
88	$H^+ + e = H + h\nu$	4.2e-7 $(300/Te)^{0.64}$	F
89	$H_2^+ + e = H + H + 10.91$ eV	2.4E-8 $(300/Te)^{0.4}$	F
90	$H_3^+ + e = H_2 + H + 9.21$ eV	2.9E-8 $(300/Te)^{0.65}$	F
91	$H_3^+ + e = H + H + H + 4.69$ eV	8.6E-8 $(300/Te)^{0.65}$	F
92	$OH^+ + e = O + H + 8.74$ eV	2E-07	K
93	$CO_2^+ + e = CO + O + 4.56$ eV	1.4E-4/Te	L
94	$N(2D) + e = N(^4S) + e + 2.38$ eV	5.5E-10 $(300/Te)^{0.5}$	C
95	$O^+(^2P) + e = O^+ + e + 5.00$ eV	4E-8 $(300/Te)^{0.5}$	C
96	$O^+(^2P) + e = O^+(^2D) + e + 1.69$ eV	1.5E-7 $(300/Te)^{0.5}$	C
97	$O^+(^2D) + e = O^+ + e + 3.31$ eV	7.8E-8 $(300/Te)^{0.5}$	C
98	$H + O_2 + M = HO_2 + M + 2.11$ eV	5.5E-32 $(300/T)^{1.6}$*[M]	B
99	$HO_2 + H = H_2O + O + 2.34$ eV	8.1E-11 × 0.02	E
100	$HO_2 + H = H_2 + O_2 + 2.41$ eV	8.1E-11 × 0.08	E
101	$HO_2 + H = OH + OH + 1.61$ eV	8.1E-11 × 0.9	E
102	$HO_2 + OH = H_2O + O_2 + 3.06$ eV	4.8E-11 exp(250/T)	E
103	$OH + O_3 = HO_2 + O_2 + 1.73$ eV	1.6E-12 exp(−940/T)	E
104	$HO_2 + O = OH + O_2 + 2.33$ eV	3E-11 exp(200/T)	E
105	$HO_2 + O_3 = OH + O_2 + O_2 + 1.23$ eV	1.1E-14 exp(−500/T)	E
106	$HO_2 + HO_2 = H_2O_2 + O_2 + 1.71$ eV	2.3E-13 exp(600/T)	E
107	$H_2O_2 + OH = HO_2 + H_2O + 1.35$ eV	2.9E-12 exp(−160/T)	E
108	$H_2O_2 + O = HO_2 + OH + 3.44$ eV	1.4E-12 exp(−2000./T)	E
109	$O(^1D) + O_2 = O_2(^1\Sigma_g) + O + 0.33$ eV	3.2E-11 exp(70/T) 0.75	E
110	$O(^1D) + O_2 = O2 + O + 1.96$ eV	3.2E-11 exp(70/T) 0.25	E
111	$O(^1D) + O = O + O + 1.96$ eV	8E-12	B
112	$O(^1D) + H_2 = H + OH + 1.88$ eV	1E-10	B
113	$O(^1D) + CO_2 = O + CO_2 + 1.96$ eV	7.4E-11 exp(120/T)	E
114	$O(^1D) + O_3 = O_2 + O_2 + 6.03$ eV	1.2E-10	E
115	$O(^1D) + O_3 = O_2 + O + O + 0.87$ eV	1.2E-10	E
116	$N(^2D) + CO_2 = NO + CO + 3.41$ eV	3.5E-13	M
117	$N(^2D) + N_2 = N(4S) + N_2 + 2.38$ eV	1.7E-14	M
118	$O_2(^1\Sigma_g) + N_2 = O_2(^1\Delta_g) + N_2 + 0.65$ eV	2.1E-15	E
119	$O_2(^1\Sigma_g) + CO_2 = O_2(^1\Delta_g) + CO_2 + 0.65$ eV	4.2E-13	E
120	$O_2(^1\Sigma_g) + O_3 = O_2(^1\Delta_g) + O_3 + 0.65$ eV	2.2E-11	E
121	$O_2(^1\Sigma_g) + O = O_2(^1\Delta_g) + O + 0.65$ eV	8E-14	E
122	$O_2(^1\Sigma_g) + O_2 = O_2(^1\Delta_g) + O_2 + 0.65$ eV	3.9E-17	E
123	$O_2(^1\Delta_g) + O_2 = O_2 + O_2 + 0.98$ eV	3.6E-18 exp(−220/T)	E
124	$O_2(^1\Delta_g) + N_2 = O_2 + N_2 + 0.98$ eV	1E-20	E
125	$O_2(^1\Delta_g) + O = O_2 + O + 0.98$ eV	1.3E-16	E
126	$O_2(^1\Delta_g) = O_2 + h\nu$	2.58E-4 s^{-1}	B
127	$O_2(^1\Sigma_g) = O_2 + h\nu$	0.085 s^{-1}	B
128	$N_2 + h\nu = N(^4S) + N(^2D)$		
129	$O_2 + h\nu = O + O(^1D)$		
130	$O_2 + h\nu = O + O$		
131	$O_3 + h\nu = O_2 + O(^1D)$		
132	$O_3 + h\nu = O_2 + O$		
133	$NO + h\nu = N(^4S) + O$		
134	$CO_2 + h\nu = CO + O$		
135	$CO_2 + h\nu = CO + O(^1D)$		
136	$H_2O + h\nu = H + OH$		
137	$H_2O + h\nu = H_2 + O$		
138	$H_2O_2 + h\nu = OH + OH$		
139	$O_3 + h\nu = O_2(^1\Delta_g) + O(^1D)$		
140	$N_2 + h\nu = N_2^+ + e$		
141	$N_2 + h\nu = N^+ + N(^4S) + e$		
142	$N_2 + h\nu = N^+ + N(^2D) + e$		
143	$N(^4S) + h\nu = N^+ + E$		
144	$O_2 + h\nu = O_2^+ + E$		
145	$O_2 + h\nu = O^+ + O + e$		
146	$O_2 + h\nu = O^+(^2P) + O + e$		

Table 2. (continued)

No.	Reaction	Reaction Rate, $cm^3\ s^{-1}$	Reference
147	$O_2 + h\nu = O^+(^2D) + O + e$		
148	$O + h\nu = O^+ + E$		
149	$O + h\nu = O^+(^2P) + E$		
150	$O + h\nu = O^+(^2D) + E$		
151	$NO + h\nu = NOI + E$		
152	$H_2 + h\nu = H_2^+ + E$		
153	$H_2 + h\nu = H^+ + H + e$		
154	$H + h\nu = H^+ + E$		

[a]Read 4.4E-12 as 4.4×10^{-12}. References are A, *Roble et al.* [1987]; B, *Roble* [1995]; C, *Rees* [1989]; D, *Smithtro and Sojka* [2005a]; E, *Jet Propulsion Laboratory* [1994]; F, *Yelle* [2004]; G, *Kasting and Pollack* [1983]; H, *Schunk and Nagy* [2000]; I, *Fox and Dalgarno* [1979]; J, *Nagy et al.* [1983]; K, *Kumar et al.* [1983]; L, *Barth et al.* [1992]; M, *Yung and DeMore* [1999]. T is neutral temperature, Ti is ion temperature, and Te is electron temperature. Tr = 0.5*(Ti + T). K30 = 5.2×10^{-11}*(Tr/300.)$^{0.2}$ Tr > 1500. K30 = 1.4×10^{-10}*(300/Tr)$^{0.44}$ Tr < 1500. K31 = 3.62×10^{-12}*(Ti/300.)$^{0.41}$ Ti > 1500. K31 = 1×10^{-11}*(300/Ti)$^{0.23}$ Ti < 1500. K52 = 1.533 – 12-5.92 $\times 10^{-13}$*b + 8.6 $\times 10^{-14}$*b^2, where b = T2/300, T2 = 0.6363*Ti + 0.3637*T (300 < T2 < 1700 K). K53 = 2.82×10^{-11} to 7.74×10^{-12}*a + 1.073E-12*a^2-5.17E-14*a^3 + 9.65E-16*a^4, where a = T1/300 and T1 = 0.667*Ti + 0.333*T (300 < T1 < 6000 K); k68 = k51*8/9*$\sqrt{((Ti + T/16.)/(T + Ti/16.))}$; k82 = c*0.22; k83 = c*0.42; k84 = c*0.36; c = 7.38E-8*(1200./Te)$^{0.56}$ Te >1200 K, c = 1.95×10^{-7}*(300./Te)$^{0.7}$ Te < 1200 K.

into the following time-independent density and wind equations:

$$\frac{1}{\rho}\frac{d\rho}{dr} = -\frac{1}{T}\frac{dT}{dr} + \frac{1}{m}\frac{dm}{dr} - \frac{g}{u_0^2} - \frac{u}{u_0^2}\frac{du}{dr} \tag{2}$$

$$\frac{1}{u}\frac{du}{dr}\left(1 - \frac{u^2}{u_0^2}\right) = \frac{1}{T}\frac{dT}{dr} - \frac{1}{m}\frac{dm}{dr} + \frac{g}{u_0^2} - \frac{2}{r}. \tag{3}$$

Here, $u_0^2 = kT/m$, $g = GM/r^2$, and m is mean molecular mass.

[14] If the variations of the mean molecular mass with time and space are ignored, the time-dependent energy equation can be reduced to the following equation:

$$\frac{1}{\gamma}\frac{\partial T}{\partial t} = \frac{1}{\rho C_p}\left[\frac{1}{r^2}\frac{\partial}{\partial r}\left(\kappa r^2 \frac{\partial T}{\partial r}\right) + q\right] - u\left(\frac{\partial T}{\partial r} - \frac{1}{\rho C_p}\frac{\partial p}{\partial r}\right). \tag{4}$$

Equation (4) is similar to the energy balance equation of *Yelle* [2004] and can be reduced to equation (3) of *Kasting and Pollack* [1983] in the steady state. The last term on the RHS is the adiabatic cooling term. The contributions of O, O_2, N_2, CO_2, H_2, H, and N are included in the expression of thermal conductivity κ and heat capacity C_p. Solving equations (2), (3), and (4) provides the macroscopic properties (ρ, T, u) of the background gas. Both ρ and T are fixed at the lower boundary. At the top boundary the bulk motion velocity u is associated with the escape velocities of multiple gases. Atomic oxygen is the dominant gas in the current Earth's upper thermosphere. *Smithtro and Sojka* [2005b] pointed out that the concentration of atomic nitrogen increases by a factor of 4 when increasing the solar EUV flux from that of solar maximum condition by a factor of 2. Our calculations confirms the findings of *Smithtro and Sojka* [2005b] and shows that atomic nitrogen indeed becomes a species competing with atomic oxygen for dominancy at the exobase under extreme solar EUV conditions. At each iteration T, u, and ρ are solved consecutively, and the time step size is adjusted according to the variation of T and ρ. The temperature equation (4) is solved using an implicit (reverse Euler) time stepper, whereas u and ρ are considered to be in quasi-steady state.

[15] The concentrations of chemical species in the thermosphere are important because they affect the heating and cooling functions and also the mean molecular mass, which in turn affects the mass density distribution. To obtain the concentrations of neutral long-lived species, we use the minor constituent diffusion approximation, as in the work by *Kasting and Pollack* [1983]. Treating major constituent diffusion self-consistently in a multicomponent atmosphere is quite difficult. In the minor constituent approximation, the mutual influences of the diffusion fluxes of major species on each other and on the minor gases are ignored, and so errors in the estimate of the diffusion fluxes can be induced. However, as demonstrated in section 3, this approach is adequate for the calculations of large-scale thermospheric structure. By combining the flux equation in the minor constituent approximation (equation (5)) with the continuity equation for species i in a moving atmosphere (equation (6))

$$u_i - u = -D_i\left[\frac{1}{n_i}\frac{\partial n_i}{\partial r} - \frac{1}{n}\frac{\partial n}{\partial r} + (1 - m_i/m)\frac{1}{p}\frac{\partial p}{\partial r} + \frac{\alpha_i}{T}\frac{\partial T}{\partial r}\right] - K\left[\frac{1}{n_i}\frac{\partial n_i}{\partial r} - \frac{1}{n}\frac{\partial n}{\partial r}\right] \tag{5}$$

$$\frac{\partial n_i}{\partial t} + \frac{1}{r^2}\frac{\partial}{\partial r}\left(r^2 n_i u_i\right) = P_i - L_i n_i \tag{6}$$

the following diffusion equation for species i can be derived:

$$\frac{\partial C_i}{\partial t} = \frac{m_i P_i}{\rho} - L_i C_i - \frac{1}{\rho r^2}\frac{\partial}{\partial r}\left[\rho r^2 (K + D_i)\frac{\partial C_i}{\partial r} + \rho r^2 (K + D_i)\frac{1}{m}\frac{\partial m}{\partial r} C_i + \rho r^2 \left(\tilde{H}_i - u\right) C_i\right] \tag{7}$$

Here C_i, n_i, m_i, P_i, L_i are the mass mixing ratio, number density, mass, chemical production, and chemical loss for species i. D_i is the (hard sphere) molecular diffusion

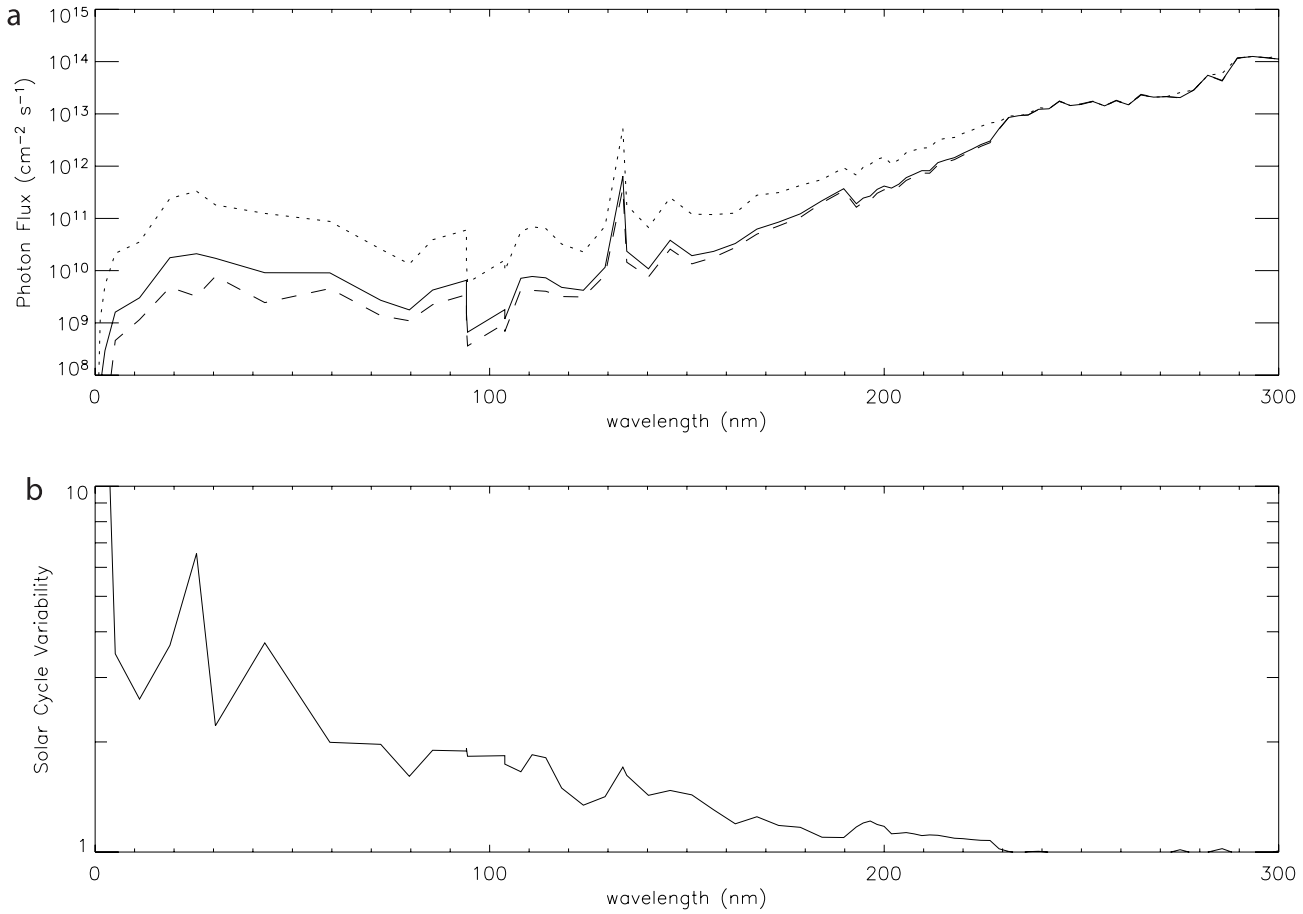

Figure 1. The solar spectrum between 0 and 300 nm and its variability during a solar cycle. (a) Photo fluxes at solar minimum (dashed), maximum (solid), and that in F107 = 3000 (dotted) conditions. (b) Ratio between solar maximum and minimum conditions.

coefficient of species i in the background gas. K is the eddy diffusion coefficient:

$$\tilde{\mathrm{H}}_i = D_i\left[(1 - m_i/m)\frac{1}{p}\frac{\partial p}{\partial r} + \frac{\alpha_i}{T}\frac{\partial T}{\partial r}\right];$$

α_{i} is the thermal diffusion factor and is set to be -0.25, -0.3, -0.4 for H, H_2, and He, respectively [*Hunten and Strobel*, 1974; *Banks and Kockarts*, 1973]. The parameter α_{i} is set equal to zero for all other long-lived species.

[16] In hydrostatic equilibrium,

$$\tilde{\mathrm{H}}_i = D_i\left[1/H_i - 1/H_a + \frac{\alpha_i}{T}\frac{\partial T}{\partial r}\right],$$

where H_i and H_a are the scale heights of species i and the background gas, respectively. The diffusion equation can be reduced to equation (25) of *Kasting and Pollack* [1983] in the steady state.

[17] For long-lived ions, the ambipolar diffusion equation [*Schunk and Nagy*, 2000] is solved. The ambipolar diffusion coefficients are calculated according to *Schunk and Nagy* [2000]. We include the contributions of 5 neutral species (O, N, H, N_2, and O_2) for the computation of the momentum transfer collision frequencies.

[18] The solar radiation spectrum used in this model extends from 0.5 nm to ~400 nm. The spectra at X-ray and EUV wavelengths (<105 nm) are from a low-resolution EUVAC model [*Solomon and Qian*, 2005]. The spectrum between 105 nm and 175 nm is from *Woods and Rottman* [2002]. The spectrum for longer wavelengths is from *Rottman et al.* [1986]. More than one activity proxy, including the 10.7 cm solar radio flux (F10.7) and its 81-d centered average ($\langle$F10.7$\rangle$), have been used in the literature to describe the variability of the solar spectrum during different phases of a solar cycle. In this paper we use the solar activity proxy P = (F10.7 + $\langle$F10.7$\rangle$)/2, defined by *Richards et al.* [1994]. Similar to *Smithtro and Sojka* [2005a], we use P = 70 for solar minimum and P = 230 for solar maximum. To scale the solar EUV flux to different conditions, we employed the low-resolution EUVAC linear scaling method of *Solomon and Qian* [2005]. We note that there are other EUV representation models which have different wavelength-dependent distributions of photons. These models and their influences on Earth's thermosphere/ionosphere have been discussed in detail by *Smithtro and Sojka* [2005a, 2005b], who found that the integrated solar EUV energy fluxes are significantly different when extrapolating these models to up to 4 times present EUV conditions. To model the thermosphere/ionosphere of early planetary atmospheres or those

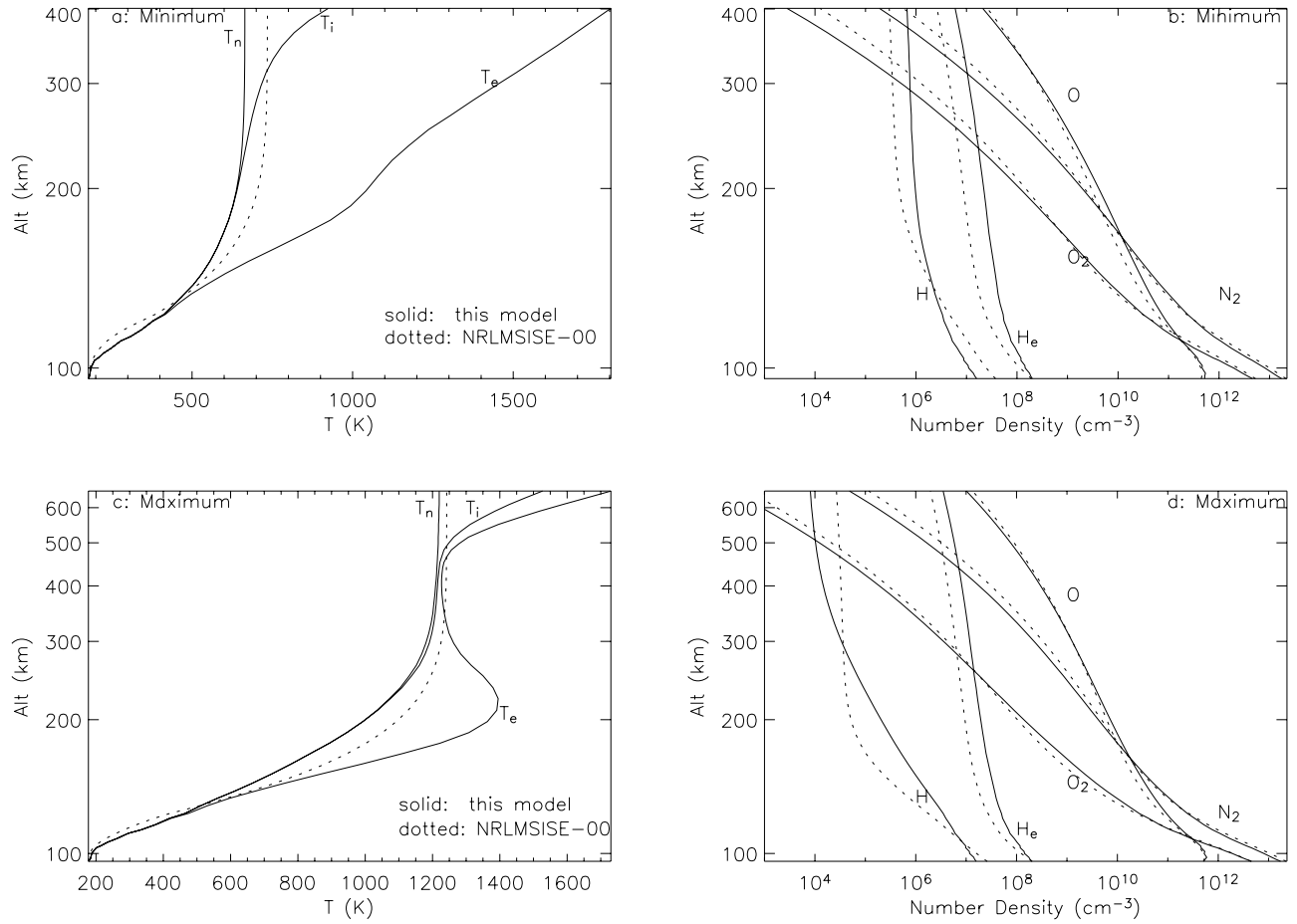

Figure 2. Temperature and number density profiles of major neutral species in solar minimum and maximum conditions. Dotted curves are the globally averaged profiles from the empirical MSIS-00 model.

in different stellar systems, observations of young stars are highly relevant, and *Ribas et al.* [2005] provide some reference EUV spectra. To investigate the responses of planetary atmospheres to different EUV representation models is beyond the purpose of this work but will be important future works. Figure 1a shows the solar spectrum at solar minimum, solar maximum, and at 20× present EUV level. Solar spectrum variability in a solar cycle is shown in Figure 1b.

[19] The 22-bin parameterization method developed by *Solomon and Qian* [2005] is used to calculate ionization and dissociation rates for O, O_2, and N_2 in the thermosphere. Ionization cross sections for N are from *Fennelly and Torr* [1992] are projected into the 22-bin scheme following the weighted (by solar EUV flux) average method of *Solomon and Qian* [2005]. The total ionization cross sections for H_2 are from *Avakyan et al.* [1998]. The dissociative ionization cross sections for H_2 are from the data of *Schunk and Nagy* [2000]. Ionization cross sections for H are assumed to be 50% those of H_2 based on the study by *Yan et al.* [1998]. These cross sections are projected into the 22-bin scheme using linear interpolation, which should introduce small errors in the present work. For H/H_2 rich atmospheres a weighted average is preferred. In this work we ignored the electron impact ionization of N, H, and H_2, which will be interesting future work.

[20] The calculations of the neutral volume heating rate q include all the neutral heating and cooling mechanisms in the global mean model for Earth's thermosphere [*Roble et al.*, 1987; *Roble*, 1995] except for the following: heating by auroral electrons, heating by gravity waves, and eddy heat conduction. The first two terms are small in the current Earth's thermosphere. The eddy heat conduction is important in the lower (<110 km) thermosphere but negligible in the upper thermosphere [*Roble et al.*, 1987. All of these energy terms are characterized by parameterizations which may or may not be applicable when extrapolated to extreme solar EUV conditions, and a full treatment is beyond the scope of this paper. The electron and ion energy considerations are similar to those in the global mean model [*Roble et al.*, 1987; *Roble*, 1995]. Because these energy treatments are described in detail by *Roble et al.* [1987] and *Roble* [1995], they are not repeated here. We only summarize the differences between this model and the global mean model of *Roble et al.* [1987] and *Roble* [1995].

[21] For the heating rates and photolysis rates in the Schumann-Runge bands of O_2, Schumann-Runge continuum of O_2, and the Hartley bands of O_3, we replaced the parameterization in the global mean model by explicit calculations of solar radiation absorption in order to facilitate the extrapolation of the model to planetary atmospheres with different composition than current Earth. Solar radia-

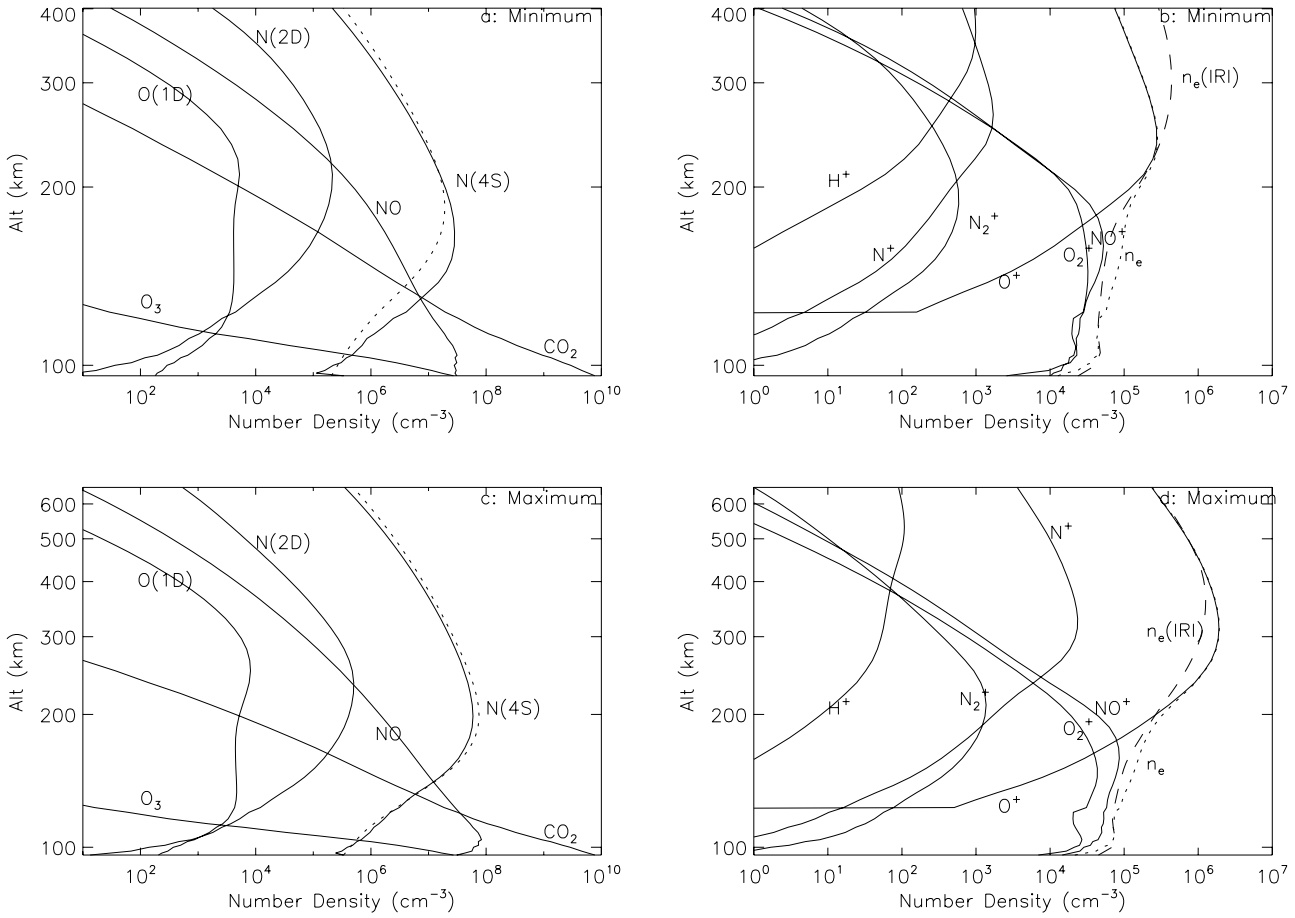

Figure 3. Number density profiles of N(^{4}S), some minor neutral species, some major ion species, and electrons in solar minimum and maximum conditions. (a and c) The dotted curves are the N(^{4}S) distributions in MSIS-00. (b and d) The dotted and the dashed curves are the electron densities calculated in the model and those obtained from globally averaged IRI model.

tion absorption by H_2O and CO_2 in the wavelength region of the Schumann-Runge bands and Schumann-Runge continuum is explicitly calculated and included in the heating and photolysis rates. Excitations of molecules/atoms by electron collision are updated according to *Schunk and Nagy* [2000]. For CO_2 cooling calculations we use the updated parameterization from *Fomichev et al.* [1998].

[22] Starting from an initial condition, the model first solves chemical equilibrium for short-lived species and then solves the diffusion equation for long-lived species using a steady state tridiagonal solver, i.e., the time derivative on the left-hand side of equation (7) is ignored. Solutions are damped by using 0.1 times the new solution plus 0.9 times the old one. Then, the sum of the mass mixing ratios of long-lived species is renormalized to unity, and the mean molecular mass is recalculated. This is preferable to calculating one species by subtraction, as the dominant species changes with altitude. The model then solves the energy equations for the electrons and the neutral gas using fixed lower boundary conditions on temperature. A zero-gradient upper boundary condition is applied for neutral gas, and a fixed downward heat flux upper boundary condition (3×10^9 eV cm^{-2} s^{-1}, the same as that in the global mean model) is applied for electrons. To solve the wind equation (3), we apply a finite (subsonic) bulk motion velocity at the top boundary, which is assessed by multiplying the Jeans escape velocities of long-lived gases by their corresponding mass mixing ratios at the exobase and then taking an average. This subsonic approach is similar to those of *Chassefière* [1996] and *Yelle* [2004] and is ideal to study the evolution of the thermospheric responses to progressively increasing solar EUV radiation. The density equation (2) is solved by fixing ρ at the lower boundary. The time step size is adjusted based on the rate of time variation of both T and ρ in order to facilitate fast convergence when the model is approaching steady state. The number densities of long-lived species are computed at the end of each iteration.

3. Model Validations

[23] Detailed comparisons of thermospheric models with the observations have been discussed extensively by *Roble et al.* [1987], *Roble* [1995], and *Smithtro and Sojka* [2005a]. Figures 2–4 show profiles of the current Earth's thermosphere under solar minimum and maximum conditions. Generally speaking, the results of our model under solar minimum and solar maximum conditions are close to those of previous works [*Roble et al.*, 1987; *Roble*, 1995; *Smithtro and Sojka*, 2005a].

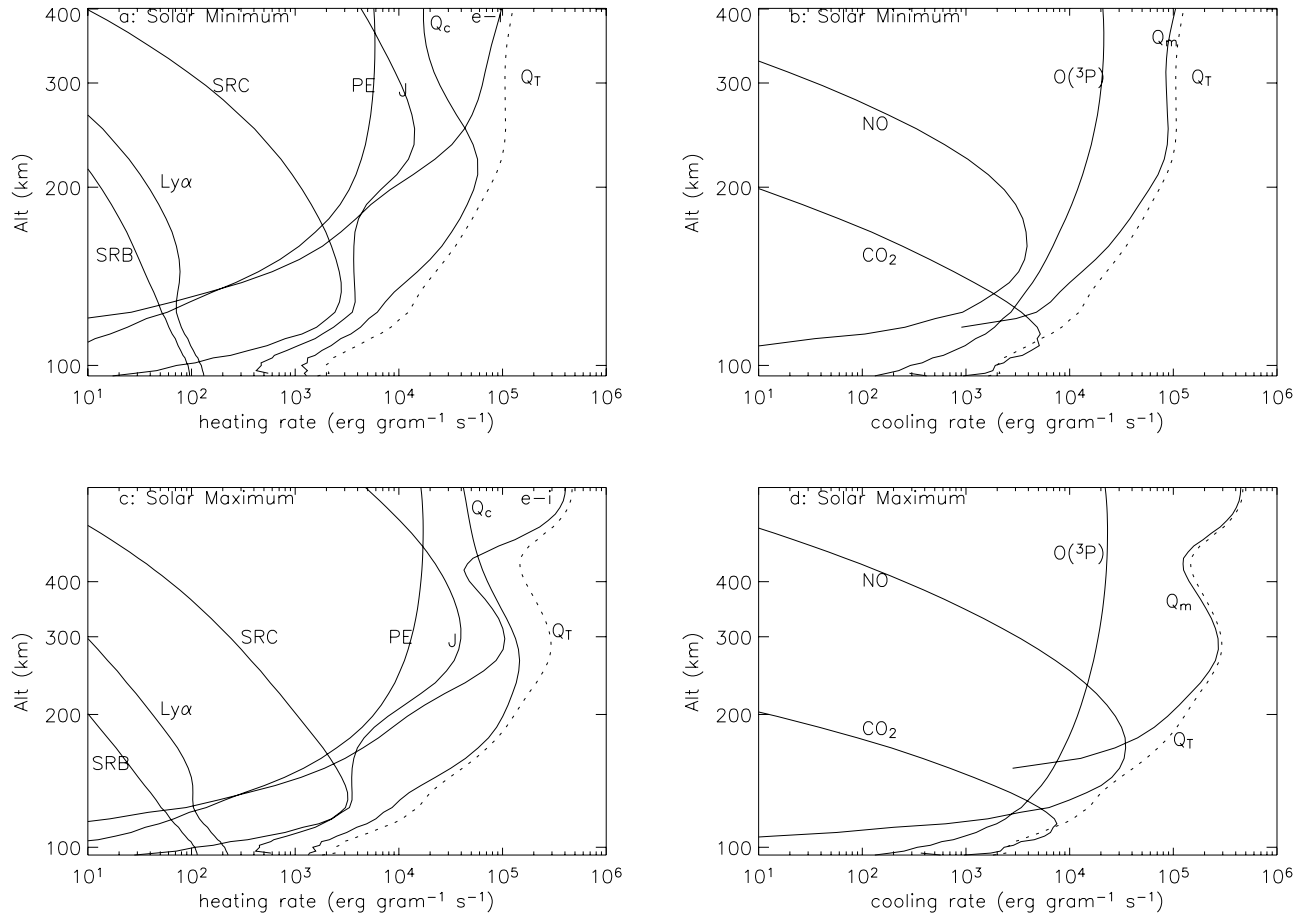

Figure 4. Heating and cooling rate profiles in solar minimum and solar maximum conditions. Q_T is the total heating rate; e-i is heating by collisions between thermal electrons, ions, and neutrals; Qc is the heating from ion-neutral and neutral-neutral chemical reactions; J is the Joule heating; PE is the direct heating from photoelectrons; SRC, SRB, and Ly α are heating from absorption in the Schumann-Runge continuum, Schumann-Runge bands, and Lyman α line, respectively; Q_m is the molecular thermal conduction cooling; O(^{3}P) is the cooling from the fine structure of atomic oxygen; NO and CO_2 are the radiative cooling from the 5.3-μm emission from NO and 15-μm emission from CO_2, respectively.

[24] Figure 2 shows the calculated neutral, ion, and electron temperature profiles, along with number density distributions of 5 long-lived species (O, O_2, N_2, He, and H) in the thermosphere. Also plotted in Figure 2 are the corresponding globally averaged profiles from the empirical MSIS-00 model. The neutral temperature profiles in the model are slightly colder than those observed. At solar minimum, the calculated exobase temperature is 671 K, as compared to 735 K in MSIS-00. At solar maximum, the exobase temperature is closer, 1220 K, compared to 1242 K in MSIS-00. The greatest discrepancy occurs at around 200 km altitude, where the model temperature is $\sim$100 K lower than that in MSIS-00. The ion and neutral temperature calculated in the model are similar to those in previous studies. At $\sim$200 km altitude, the electron temperature peak value is $\sim$1400 K, close to that of *Roble et al.* [1987]. The electron temperature at $\sim$400 km is closer to the neutral temperature than those in previous models [*Roble et al.*, 1987; *Roble*, 1995; *Smithtro and Sojka*, 2005a], probably a reflection of the stronger collisional coupling between neutrals, ions, and electrons in this model. The profiles of neutral species in Figure 2 are similar to those in MSIS-00 but the fit is not as good as those in previous works. The discrepancies may be partially caused by the minor constituent approximation employed in the diffusion equation.

[25] Figures 3a and 3c show the calculated profiles of 3 long-lived species (NO, N(^{4}S), and CO_2) and 3 short-lived species (O_3, O(^{1}D), and N(^{2}D)) at solar minimum and solar maximum. These species are closely related to the heating and/or cooling calculations in the model. All species have profiles similar to those in previous works [*Roble et al.*, 1987; *Roble*, 1995; *Smithtro and Sojka*, 2005a]. The dotted curves are the N(^{4}S) density profiles from MSIS-00. The model calculated N(^{4}S) density profile is closer to that in MSIS-00 at solar maximum than at solar minimum. The densities of N(^{4}S), N(^{2}D), and O(^{1}D) are greater at solar maximum than at solar minimum due to stronger photodissociation rates. Figures 3b and 3d show the model calculated electron density profiles (dotted curves) and the profiles of 5 ion species (O^+, NO^+, O_2^+, N^+, H^+, and N_2^+) at solar minimum and at solar maximum. As found in previous works [*Donahue*, 1968; *Brinton et al.*, 1969; *Hoffman et al.*, 1969; *Roble et al.*, 1987; *Roble*, 1995; *Smithtro and Sojka*, 2005a], O^+ is the dominant ion species

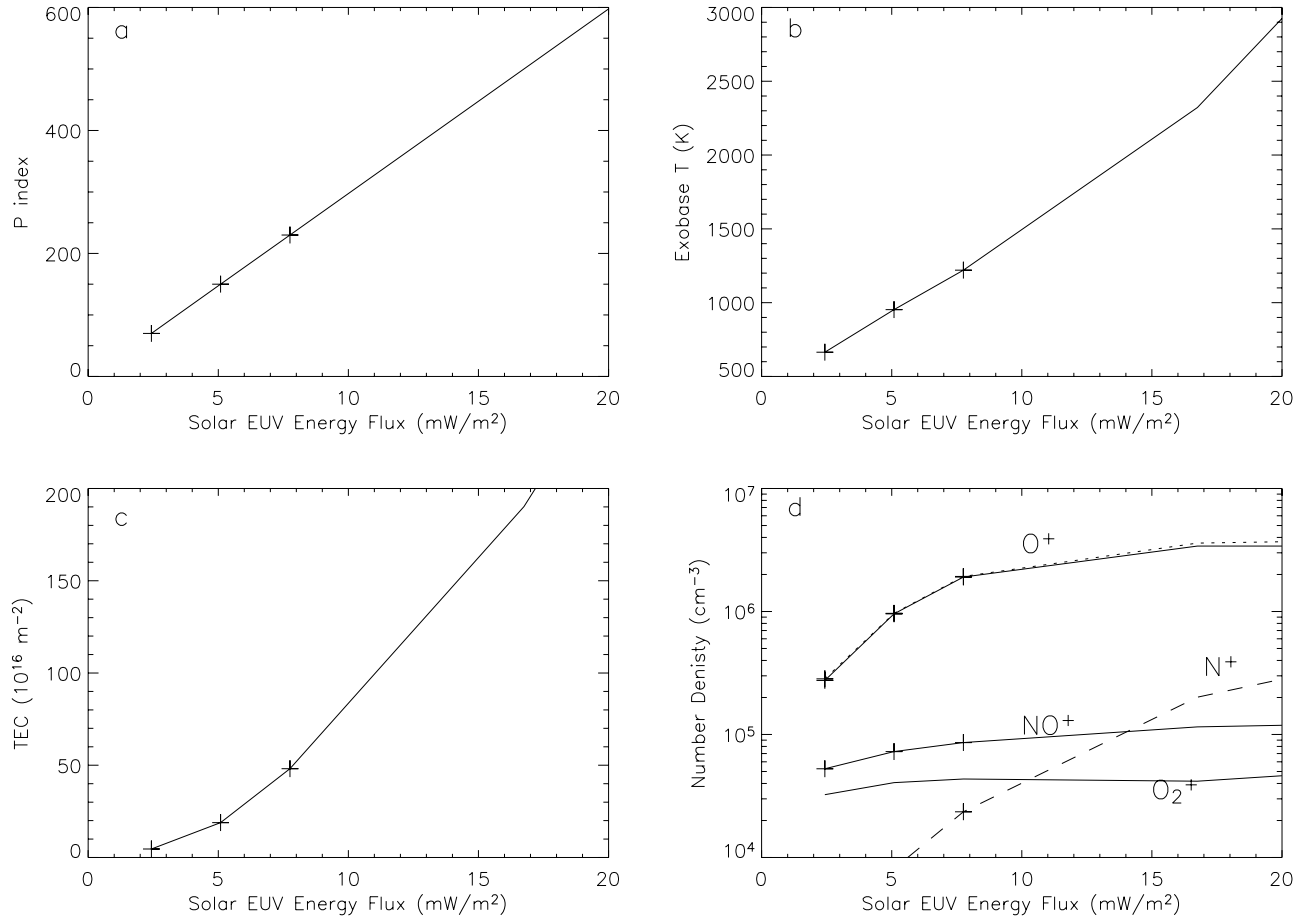

Figure 5. (a) Variations of solar EUV energy flux with P index. (b) Variation of exobase temperature with solar EUV flux. (c) Variation of TEC with solar EUV flux. (d) Variation of peak densities of major ion species with solar EUV flux. The dotted curve in Figure 5d marks the variation of peak electron densities. In Figures 5a–5d the crosses correspond to the solar minimum, mean, and maximum values.

at high altitudes, and both O_2^+ and NO^+ dominate at low altitudes. The peak electron densities at solar minimum and maximum are $\sim 3 \times 10^5$ cm^{-3} and $\sim 2 \times 10^6$ cm^{-3}, respectively Figure 3b and 3d also show the empirical electron density profiles (dashed curves), which are obtained by taking the global average of data from the International Reference Ionosphere model [*Bilitza*, 1991, 2001] under corresponding solar EUV fluxes. The model calculated electron density profile agrees well with that in the empirical profile under solar maximum conditions. The agreement is not as good under solar minimum conditions, especially at altitudes greater than 300 km. An important feature of the Earth's ionosphere is its short timescale, which leads to strong diurnal and latitudinal variations of electron density profiles. Thus, it is to be expected that the results from 1-D models differ from the global averaged values in empirical model such as IRI.

[26] The total heating and cooling profiles, as well as the contributions from important individual mechanisms, are plotted in Figure 4. The general shapes of these heating/cooling profiles and the importance of each heating/cooling mechanism are similar to those of *Roble et al.* [1987] and *Roble* [1995]. At solar minimum, the dominant heating mechanism above ~250 km is the collisional heating by ambient electrons (e-i), followed by the heating by exothermal chemical reactions (Q_c), which includes neutral-neutral and neutral-ion reactions. Between 190 and 250 km, chemical heating is dominant, followed by electron collision heating. Below 190 km, chemical heating is still dominant but Joule heating becomes the second most important heating mechanism, with a peak contribution of ~30% at 110 km altitude. Heating from O_2 absorption in the Schumann-Runge continuum begins to be important below ~150 km and reaches a peak of ~20% at 120 km. The dominant cooling mechanism at high altitudes is molecular thermal conduction, supplemented by less than a 20% contribution from atomic oxygen fine structure cooling (63 μm) at ~300 km. The dominant cooling agent at low altitudes is CO_2 through 15-μm IR radiation, which contributes ~10% to the total cooling at ~130 km and more than 90% below 110 km. NO contributes (~15%) to the total cooling rate at ~145 km through 5.3-μm non-LTE radiation. At solar maximum the most apparent change in the heating/cooling profiles, other than the overall increase of total heating/cooling, is the increased cooling contribution of NO in the lower thermosphere, which reaches ~80% at ~140 km. Previous work [*Roble et al.*, 1987] has found the same dominant role of NO cooling at similar altitude at solar maximum. In general, contributions from different heating/

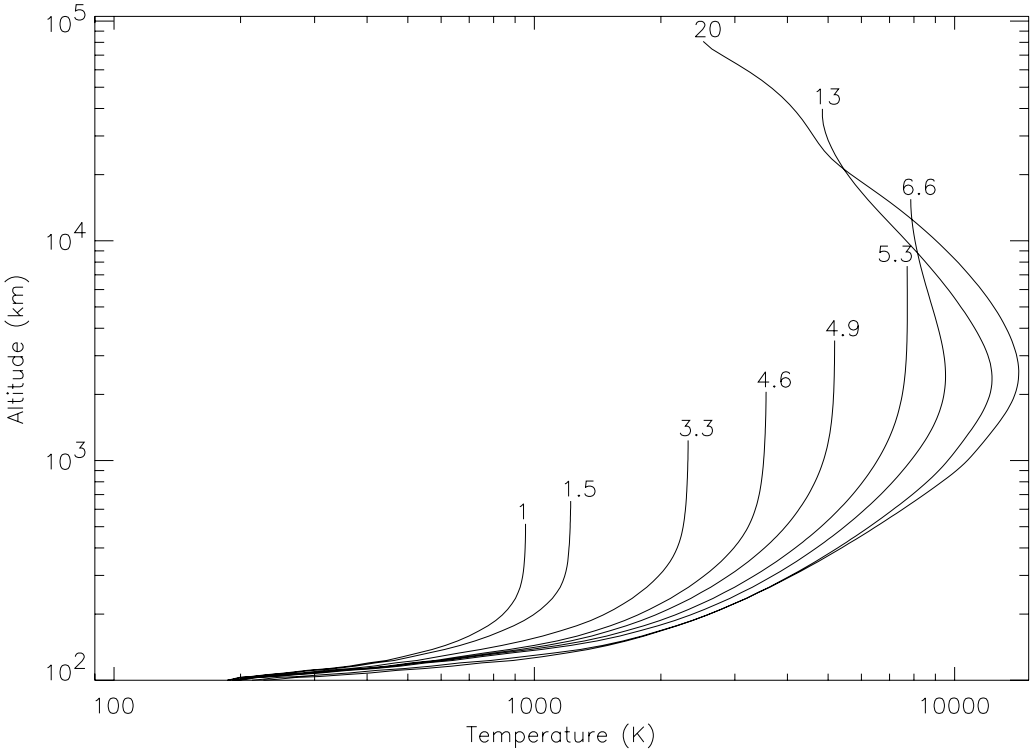

Figure 6. Temperature profiles for different solar EUV flux cases (normalized to present-day solar mean energy flux ~1 times present EUV, which represents solar EUV energy flux ~5.1 mW/m^2). It is shown that when solar EUV energy flux exceeds certain critical value, the upper part of the thermosphere begins to cool as a result of the increasingly significant adiabatic cooling effect. Beyond the critical flux (~5 times present EUV in this plot), the higher the energy input into the thermosphere, the lower the exobase temperature. This behavior is typical in the studies of hydrodynamic flow in planetary atmospheres.

cooling mechanisms in this model at both solar minimum and solar maximum are close to those in previous works.

[27] *Smithtro and Sojka* [2005b] discussed the response of the Earth's ionosphere and thermosphere under extreme solar cycle conditions (EUV energy flux between 0.5 and 14.5 mW/m^2) using their GAIT (global average ionosphere and thermosphere) model. Figure 5a shows the relationship between the P index and the solar EUV energy flux. The energy fluxes corresponding to solar minimum, mean, and maximum are marked by crosses. Figures 5b and 5c show the variations of the exobase temperature and the total electron content (TEC) with solar EUV flux. We note that the exobase temperature computed in this model is a slightly better linear function of the solar EUV flux in the energy flux range 2 to 15 mW/m^2 than that in GAIT. For stronger solar EUV fluxes, the exobase temperature begins to show nonlinearity in a similar way, as demonstrated in GAIT. The TEC calculated in the model increases from ~4.6 TEC units under solar minimum condition to ~48 TEC units under solar maximum condition (1 TEC unit = 10^{16} electrons/m^2). TEC calculated in the present model increases faster with increasing solar EUV fluxes than the GAIT model and has similar TEC values as that in the GAIT model (19 TEC units) under solar mean condition. Figure 5d shows the peak density variations of 4 ion species (O^+, N^+, NO^+, and O_2^+) and electrons with solar EUV flux. These are good indicators of the behavior of the ionosphere in the model. In GAIT, the peak density of O^+ reaches a local maximum at a solar EUV energy flux of ~11 mW/m^2 and decreases slightly for stronger solar EUV fluxes. *Smithtro and Sojka* [2005b] examined the plateau feature and suggested that competing factors in both the production and loss of O^+ are responsible. Our model confirms the slower increase of the O^+ peak density when the solar EUV flux increases beyond ~10 mW/m^2. The peak densities of O^+ and N^+ in our model are less than a factor of 2 greater than those in GAIT when the solar EUV energy flux reaches 15 mW/m^2. *Smithtro and Sojka* [2005b] observed that the concentration of atomic nitrogen increases by a factor of 4 when the solar EUV flux is increased by a factor of 2 from that at solar maximum and attributed this change to the increased photodissociation of N_2 and accelerated production of N through ion-neutral chemical reactions. Our calculations confirm this finding. In general, the behavior of the thermosphere/ionosphere in our model is similar to that in GAIT [*Smithtro and Sojka*, 2005b].

4. Thermosphere Expansion Under Extreme Solar EUV Conditions and the Adiabatic Cooling Effect

[28] In the previous section the model was validated against the current Earth's thermosphere through comparison with observations and previous models. In this section

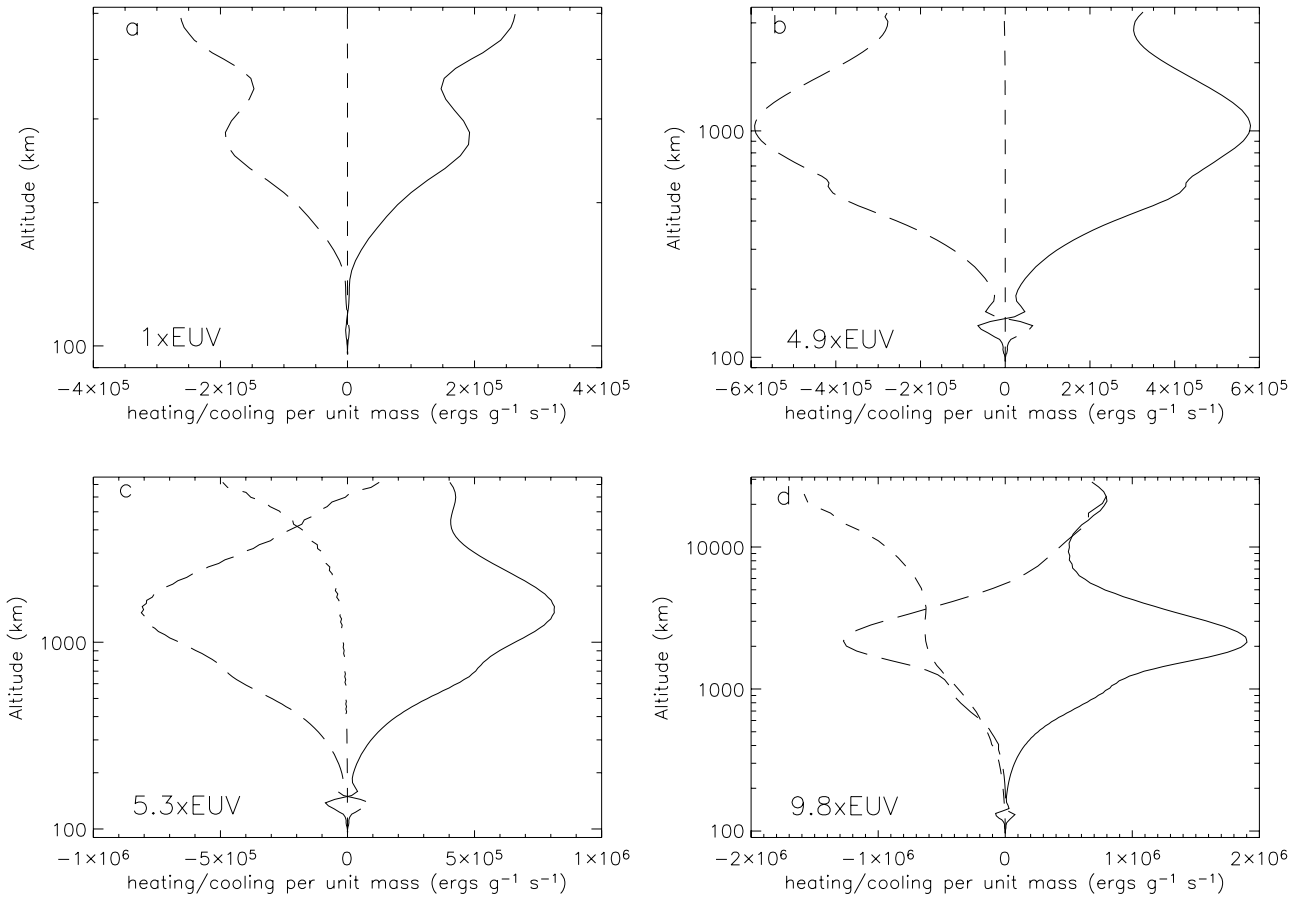

Figure 7. Profiles of heating and cooling mechanisms under different solar EUV flux cases (normalized by the solar EUV energy flux at solar mean). The solid curves are the net heating from radiative transfer calculations, including both the heating terms and IR cooling terms described in section 3. The long dashed curves are the molecular thermal conduction, and the short dashed curves are the adiabatic cooling.

we subject the model to much stronger solar EUV radiation levels.

[29] Figure 6 shows the temperature profiles of the thermosphere under different solar EUV fluxes. When the energy input into the thermosphere/ionosphere system increases, the exobase expands. The response of the temperature profile is more complicated. For solar EUV fluxes smaller than ~5 times that of today (5 × EUV or ~25 mW/m^2), the peak temperature in the thermosphere occurs at the exobase level. For solar EUV fluxes greater than ~5 × EUV, the peak temperature still increases with energy flux, but the upper part of the thermosphere begins to cool as a result of the increasingly significant adiabatic cooling effect. The higher the energy input into the thermosphere, the lower the exobase temperature. This behavior is typical in hydrodynamic models of planetary atmospheres [*Watson et al.*, 1981; *Kasting and Pollack*, 1983; *Chassefière*, 1996; *Yelle*, 2004; *Tian et al.*, 2005a, 2005b].

[30] The significance of the adiabatic cooling effect is better illustrated in Figure 7, where three heating/cooling mechanisms are plotted as functions of altitude. Figures 7a–7d correspond to the situations for four solar EUV flux levels: 1, 4.9, 5.3, and 9.8 times the present value of 5.1 mW/m^2. The solid curves are the net heating profiles from radiative transfer calculations, which include all radiative heating mechanisms and all the IR cooling mechanisms described in previous sections. The long dashed curves represent molecular thermal conduction, and the short dashed curves represent adiabatic cooling. It is clear that when solar EUV flux is smaller than ~4.9 times present EUV, all through the system the net heating from radiative transfer calculations is balanced by thermal conduction. Adiabatic cooling is negligible because of the small bulk motion velocities. In the 5.3 times present EUV case, adiabatic cooling becomes effective near the exobase, and the significance of thermal conduction cooling begins to decrease. As the energy flux continues to increase, the adiabatic cooling effect becomes greater, and the temperature begins to decrease with altitude in the upper part of the thermosphere. In the large solar EUV flux cases, thermal conduction acts to heat the uppermost part of the thermosphere (comparable to the heating from radiative transfer processes) rather than cooling it.

[31] In Figure 8 we plot the exobase temperature, peak temperature, exobase altitude, and exobase bulk motion velocity as a function of solar EUV fluxes (normalized by the solar mean EUV flux). Figures 8a–8d suggest that the

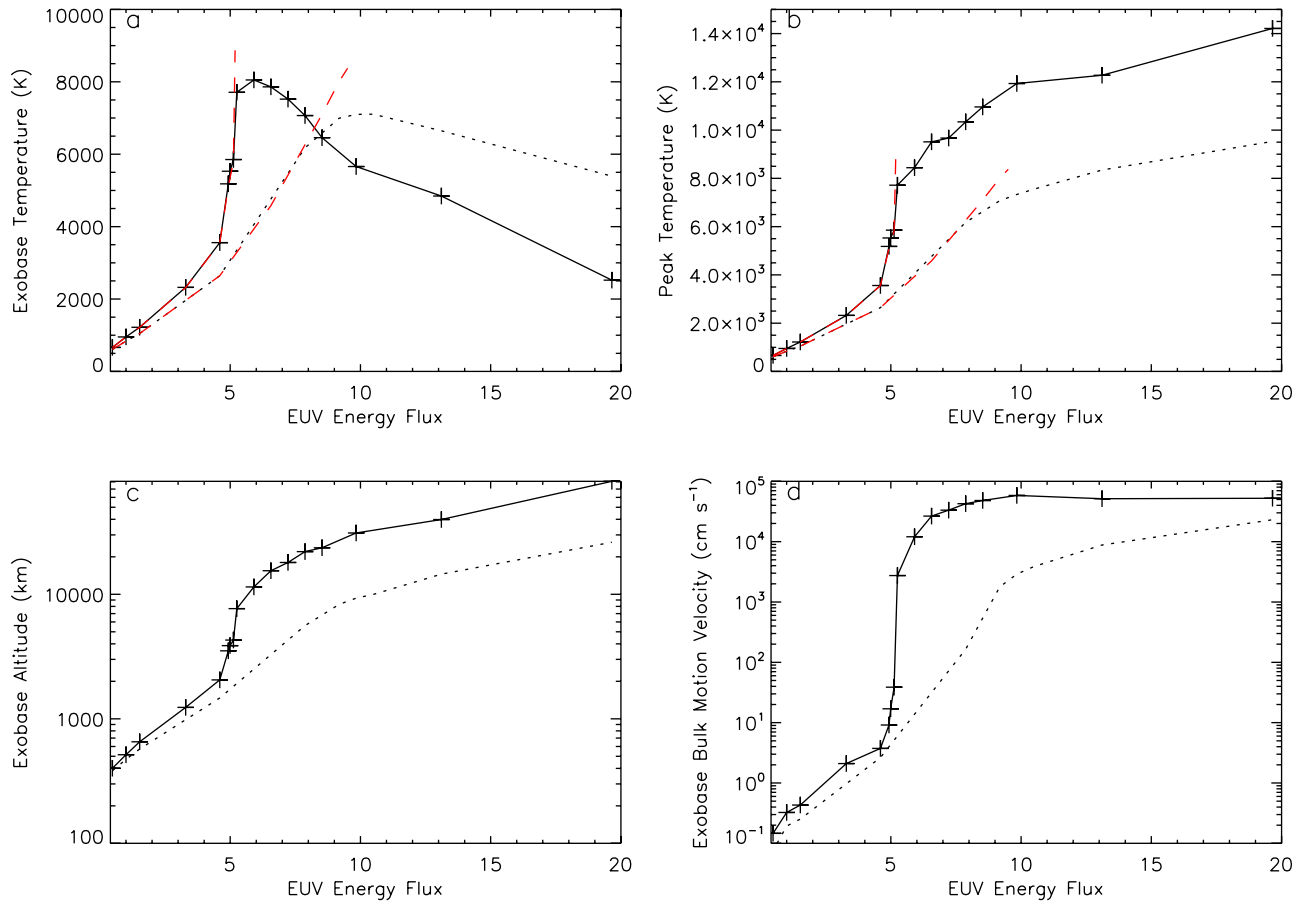

Figure 8. Variation of (a) exobase temperature, (b) the peak temperature, (c) altitude, and (d) bulk motion velocity with solar EUV flux. In Figures 8a–8d, the values on the horizontal axis are normalized by the solar EUV flux at solar mean. The dotted curves in Figures 8a, 8b, and 8c are obtained by fixing the electron temperature to be the same as the neutral temperature. The red, dashed curves in Figures 8a and 8b are obtained by forcing hydrostatic equilibrium.

response of the Earth's thermosphere to extreme solar EUV conditions can be divided into the two regimes defined in the introduction section by a critical solar EUV flux (~5 times present EUV for the solid curve). In regime I (hydrostatic equilibrium), the thermosphere behaves similarly to that demonstrated by the GAIT model and by our model in previous section. The peak temperature occurs at the exobase. Both the temperature and altitude at the exobase level increase nonlinearly with the solar EUV flux. Analysis of our simulation results shows that atomic oxygen maintains its status as the dominant species at the exobase in regime I, with increasingly stronger competition from atomic nitrogen. Indeed, the number density of atomic nitrogen becomes comparable to that of atomic oxygen at the exobase at a solar EUV flux close to 5 times present EUV.

[32] The thermosphere enters regime II (hydrodynamic flow) when the solar EUV flux increases beyond the critical flux. In this regime, the peak temperature no longer occurs at the exobase, and the exobase temperature decreases with increasing solar EUV flux. The altitude and the bulk motion velocity at the exobase level, as well as the peak temperature, increase with slopes much lower than those near the end of regime I. Atomic nitrogen becomes the dominant species at the exobase and ions (O^+ dominant) become increasingly important and eventually dominate the exobase.

[33] The behavior of the bulk motion velocity at the exobase level changes more dramatically at the transition from regime I to regime II (Figure 8d). Simulations show that the bulk motion velocity at the exobase increases from <10 cm/s to >10^3 cm/s when the P index is changed from 750 (4.9 times present EUV or energy flux = 25.1 mW/m^2) to 800 (5.3 times present EUV or energy flux = 26.7 mW/m^2). This dramatic increase of the bulk motion velocity at the exobase is controlled by the fast increase of exobase temperature from ~5000 K to nearly 8000 K. More discussion on this transition will follow in section 5.

[34] As discussed in section 3, the dominant heating mechanism for the upper thermosphere during a normal solar cycle is the electron collision heating of the neutral gases. Analysis of the energy budget of the thermosphere under extreme solar EUV fluxes suggests that the electron collision heating maintains its status as the dominant heating mechanism in the upper thermosphere. Because the electron collision heating depends on the temperature difference between the electrons and the neutrals, a correct

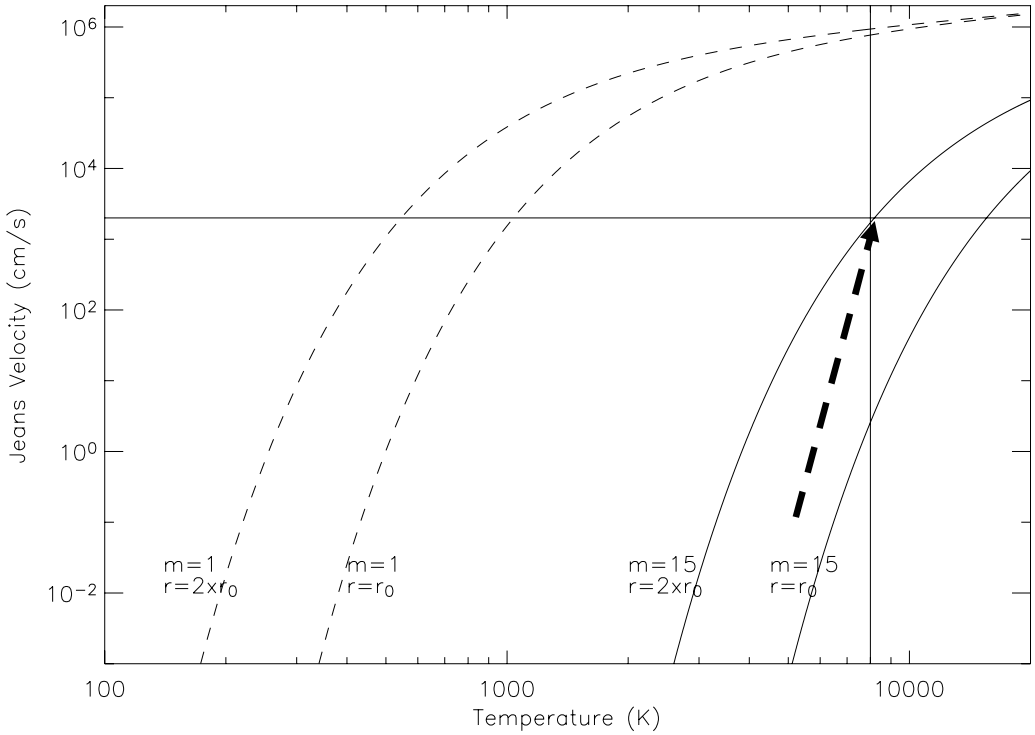

Figure 9. Jeans escape velocity as a function of exobase temperature. The solid curves are for a hypothetical gas with molecular weight 15. The dashed curves are for atomic hydrogen. For each gas, two curves are plotted, corresponding to two different exobase altitudes, one at the surface of the Earth, the other at 2 Earth radii. The dashed arrow mark is discussed in section 5.

solution of the electron temperature is critical in accurately calculating the electron collision heating. In this model we solve the energy equation of the electrons by assuming that the electrons are static, i.e., the adiabatic cooling effect is ignored for electrons. This will cause an overestimation of the electron temperature and their contribution to neutral heating. To estimate how the adiabatic cooling for electrons could have influenced the response of the Earth's thermosphere under extreme solar EUV conditions, a series of simulations was done by fixing the electron temperature to the neutral temperature, which sets the electron collision heating to zero. The simulation results are plotted in Figure 8 as dotted curves. These sensitivity tests suggest that the thermosphere expansion could occur in a much more moderate style. A critical flux ($\sim$10 times present EUV or energy flux = $\sim$50 mW/m^2) can still be found beyond which the exobase would begin to cool when the solar EUV flux is further increased.

[35] To better understand the influence of the adiabatic cooling effect, we forced the thermosphere to be in hydrostatic equilibrium by imposing a small bulk motion velocity at the exobase level. The red, dashed curves in Figures 8a and 8b represent the variation of the exobase temperature and peak temperature with varying solar EUV fluxes. Our simulations show that the thermosphere's response remains the same when solar EUV flux is small – the hydrostatic equilibrium assumption is sound when the energy input into the thermosphere is limited. But as the solar EUV flux approaches the critical flux, the exobase begins to expand and warm up dramatically. When the exobase altitude and temperature increase, the atmospheric blowoff state is quickly reached, and eventually the exobase vanishes. This explosive expansion of the exobase is accompanied and caused by the extremely high exobase temperature, which is consistent with the accelerated trend of the exobase temperature growth under smaller energy inputs. These sensitivity test results suggest that the Earth's thermosphere could experience a fast transition into the atmospheric blowoff state when exposed to certain critical solar EUV conditions, and that hydrostatic equilibrium does not apply in those cases.

[36] The Jeans escape parameters at the exobase under different solar EUV conditions can be evaluated from Figures 8a and 8c. Analysis shows that under no solar EUV conditions do the exobase parameters satisfy the atmospheric blowoff criteria ($\lambda_c < 1.5$).This shows that (1) planetary atmospheres can be in the hydrodynamic flow regime without satisfying the blowoff criteria and (2) adiabatic cooling associated with the hydrodynamic flow in planetary thermospheres actually prevents the atmosphere from reaching the blowoff state.

5. Discussion

[37] As described in last section, when the P index increases from 750 (4.9 times present EUV) to 800 (5.3 times present EUV), the exobase temperature climbs from $\sim$5000 K to $\sim$8000 K (Figure 8a), and the exobase moves from $\sim$3500 km altitude to $\sim$7700 km. At the same time, the bulk motion velocity jumps from <10 cm/s to >10^3 cm/s. This dramatic change in the bulk motion velocity at the exobase (which marks a transition from static thermosphere

to hydrodynamic flow) is a consequence of the exponential dependence of the Jeans escape velocity on the exobase temperature and exobase altitude. In Figure 9 we plot the variations of the Jeans escape velocities as a function of exobase temperature. The two solid curves (for exobase at 1 Earth radius and 2 Earth radii, respectively) are for a hypothetical gas with molecular weight 15, which is the same as the background gas (dominated by atomic O and N) at the exobase in our model at high solar EUV conditions. Because the exobase level moves outward when the solar EUV flux increases, the actual direction in which the Jeans velocity grows is marked by a symbolic arrow, whose sharp slope is the cause of the dramatic increase of the bulk motion velocity in Figure 8d.

[38] Figures 8a and 8d suggest that for a thermosphere with current Earth's specifications, the velocity range in which hydrodynamic flow begins to be important is between 100 and 1000 cm/s. The corresponding temperature range is between 7000 K and 8000 K. It is interesting to note that if the Earth's thermosphere were dominated by light gases, such as atomic hydrogen, an exobase temperature less than 1000 K would be adequate to generate a Jeans escape velocity of ~1000 cm/s (dashed curves in Figure 9). Thus, if the early Earth's atmosphere were dominated by hydrogen, as suggested by *Tian et al.* [2005b], the exobase and peak temperature in the thermosphere would have been lower than ~1000 K. This hypothesis is in agreement with the hydrodynamic models for early Earth and Venus [*Watson et al.*, 1981; *Kasting and Pollack*, 1983; *Chassefière*, 1996; *Tian et al.*, 2005b]. We note that all transonic (and some subsonic) hydrodynamic models [*Watson et al.*, 1981; *Krasnopolsky*, 1999; *Tian et al.*, 2005a, 2005b; *Tian and Toon*, 2005; *Strobel*, 2007, 2008] extend beyond the exobase level in the corresponding planetary atmospheres, where the hydrodynamic equations are invalid. Comparisons between the hydrodynamic fluxes with the Jeans escape fluxes in more than one case show that Jeans escape is orders of magnitude smaller than the hydrodynamic flow. If Jeans escape is the only mechanism to remove the gases, hydrodynamic fluxes need to be reduced from the values obtained from the hydrodynamic models, which will result in an increase of exobase temperature and density until the Jeans escape fluxes are comparable to the hydrodynamic fluxes. This regulating process suggests that the hydrodynamic flow rate is an upper limit to the physical escape rate. Nonthermal escape fluxes also depend on the density of escaping species at the exobase, and thus similar feedback will occur, although the picture becomes more complicated.

[39] *Bougher et al.* [1999, 2002] proposed that the adiabatic cooling and heating effects of thermospheric circulations play roles of thermostat in the heat budgets of present terrestrial thermospheres. In our 1-D model, the whole thermosphere is expanding under extreme solar EUV radiation and the adiabatic cooling associated with the hydrodynamic flow plays a similar thermostat role, and could have protected the atmospheres from atmospheric blowoff at early stages of Solar System history when the solar EUV flux was very high. More simulations will be needed to better evaluate this thermostat effect and to determine how low Earth's exobase temperature may have been in the distant past.

[40] In this model the bulk motion velocity is associated with the Jeans escape velocities of multiple gases at the exobase. In reality nonthermal escape processes are significant in atmospheric escape from terrestrial planets today. Our simulations suggest that the thermosphere of a hypothetical early Earth (with the same composition as that of today) could have expanded to beyond the present Earth's magnetopause (~10 Earth radii), in which case strong nonthermal escape processes similar to those simulated by *Lammer et al.* [2007] for extended thermospheres of Venus-like, CO_2-rich extrasolar planets could occur. We note that the location of the magnetopause in the *Lammer et al.* [2007] model is determined by balancing the ram pressure of a much stronger solar wind with the magnetic fields of slowly rotating Earth-like extrasolar planets around low-mass M stars. For a rapidly rotating planet, its intrinsic magnetic field could be significantly stronger. In addition, the plasma density in the magnetosphere of early terrestrial planets could be significantly greater than that of today due to the greater flux of ionizing radiation from young stars. Thus the pressure of the magnetospheric plasma could have helped to balance the solar wind. These factors should all be studied in future work. It will clearly be important to include the effect of nonthermal escape processes when evaluating the total escape rate from early terrestrial planets. But from the perspective of thermosphere energy balance, including any additional nonthermal escape processes is equivalent to increasing the bulk motion velocity at the exobase, which enhances the hydrodynamic flow in the thermosphere and makes the adiabatic cooling effect more prominent. The exobase temperature could therefore be lowered even further if nonthermal escape were taken into account. Thus the thermostat role of the hydrodynamic flow will be strengthened by the inclusion of nonthermal escape processes.

[41] We note that our simulation results with forced hydrodynamic equilibrium are in rough agreement with the hydrostatic thermosphere models of *Kulikov et al.* [2007] for EUV flux values up to ~5 times present EUV, except that Figure 3 of *Kulikov et al.* [2007] seems to indicate that an exobase is always available in the solar EUV flux range between 1 times present EUV and 100 times present EUV, while our model runs into atmospheric blowoff. The locations of the exobase of a planetary atmosphere with low CO_2 content under different solar EUV conditions are not reported by *Kulikov et al.* [2007]. The Kulikov et al. model solves the heat balance equation by including the vibrational kinetics of radiating molecules (CO_2, NO, CO, O_3, OH, etc.) as well as the 63-μm O line. *Kulikov et al.* [2007] also included an eddy thermal conduction cooling function and a heating function due to dissipation of turbulent energy. Because the heating and cooling profiles were not provided by *Kulikov et al.* [2007], it is difficult to directly compare our results with theirs. The IR cooling agents in our model (15-μm CO_2, 5.3-μm NO, and 63-μm O) have been generally accepted as the dominant radiative cooling agents in the thermospheres of the Earth, Mars, and Venus [*Gordiets et al.*, 1982; *Roble et al.*, 1987; *Roble*, 1995; *Bougher et al.*, 2002]. Further work is needed to determine whether or not the IR radiation from the other minor radiatively active molecules can be the

cause of the discrepancy. For EUV fluxes greater than 5× present EUV, hydrodynamic flow and adiabatic cooling take place so that the Kulikov et al. model is no longer valid. Despite the difference in finding the exobase under extreme solar EUV fluxes, the fact that extremely high exobase temperatures are given by *Kulikov et al.* [2007] for greater than 5 times present EUV supports our conclusion that hydrodynamic flow (driven by fast Jeans escape of major gases at the exobase level) should start, and the adiabatic cooling effect should be significant when Earth's thermosphere is exposed to extreme EUV radiation levels.

[42] *Kulikov et al.* [2007] did recognize the possible cooling effect of fast Jeans escape of hydrogen on the energy budget of the thermosphere. The simulations in this paper suggest that even if the Earth's atmosphere were "dry," hydrodynamic flow and the associated adiabatic cooling could still be significant. Recent calculations for early Venus [*Kulikov et al.*, 2006] and Venus-like extrasolar planets in the habitable zones of M stars [*Lammer et al.*, 2007] show that the exobase temperatures could reach more than 8000 K when exposed to 100× present EUV level. Figure 6 suggests that these planetary thermospheres may be in the hydrodynamic flow regime. It is possible that stronger radiative cooling from more abundant IR agents and/or stronger gravity of more massive terrestrial planets may keep their thermospheres in hydrostatic equilibrium. Because the composition of the atmosphere modeled in this paper is the same as that of present Earth, the relative importance of the adiabatic cooling and the CO_2 cooling for CO_2-rich planetary atmospheres (the topic of a future paper) is not discussed here. However, it is reasonable to conclude that a broad range of terrestrial planets (in and out of the solar system) are in the hydrodynamic flow regime during certain stages in their evolutionary history. Without including the adiabatic cooling effect, the thermospheric structures of these terrestrial planets cannot be predicted accurately, and the derived escape rates of atmospheric gases from these planets might be flawed.

[43] A fixed, downward heat flux from the plasmasphere is assumed for the electron gas. By doubling this heat flux in the 10 times present EUV case, the exobase density and neutral gas temperature change by less than 5%.

[44] The Joule heating term in the model is included by specifying an externally applied electric field (assumed constant with height) and calculating the Pedersen conductivity. Similar to that in the global mean model, a fixed E field is used for all model runs. Because the Pedersen conductivity increases and the atmosphere expand when increasing solar EUV energy input, the Joule heating contribution increases in magnitude. Simulations by increasing or decreasing the Joule heating term by a factor of 2 in the 10× present EUV case show that the model is not sensitive to the Joule heating, which is in agreement with the relatively insignificant (<1% in most part of the thermosphere) contribution of Joule heating to the total heating budget.

[45] In this paper we have concentrated on calculating the response of present Earth's thermosphere under extreme solar EUV conditions. The composition of early Earth's atmosphere almost certainly was different from that of today and this composition change could have had significant impacts on the structure of both the lower and the upper atmosphere. Thus the fixed lower boundary temperature and density used in all simulations in this work should be considered as an approximation. To explore how the variations of the lower boundary conditions will influence the thermosphere/ionosphere is beyond the scope of this manuscript. Thus, the details (such as what the critical solar EUV flux might have been, what the exobase temperature was, etc.) of how the Earth's thermosphere actually evolved in time will require future work.

[46] By exposing the Earth's upper atmosphere to extreme solar EUV conditions, extremely high neutral, ion, and electron temperatures are obtained in the model. Therefore, there are many uncertainties. Are there important radiative cooling agents other than the three radiative cooling terms in this work? Are the temperature dependences of the reaction rate coefficients, which were fit over a narrower range, applicable to the high-temperature situations? These questions cannot be addressed by the present model and require future work and cautious reading of the results in this paper. We note that the transition temperature (which itself depends on the composition of the atmosphere and can be affected by possible efficient nonthermal escape processes) from regime I to regime II of planetary atmospheres should be more important than the critical solar EUV flux, which is likely to change considering the model uncertainties.

[47] The model developed in this work provides a good framework upon which future researches can be done to study the long-term evolution of planetary atmospheres under various solar radiation conditions. Applying the model to terrestrial-like extrasolar planets, including water planets, will be interesting and important future work.

6. Conclusions

[48] In this work we developed a multicomponent hydrodynamic thermosphere model to self-consistently study the Earth's thermosphere under extreme solar EUV conditions. The model was validated against observations (MSIS-00) and models [*Roble et al.*, 1987; *Roble*, 1995; *Smithtro and Sojka*, 2005a] of the Earth's present thermosphere. The model also agrees with theoretical models developed for moderately strong solar EUV fluxes [*Smithtro and Sojka*, 2005b]. In this paper we concentrate on the response of the Earth's thermosphere (with its current composition) to extreme solar EUV conditions. The model shows the following:

[49] 1. The Earth's thermosphere could experience a fast transition into atmospheric blowoff state if hydrostatic equilibrium is forced in the model. The transition occurs at certain critical solar EUV fluxes, the value of which depends on the treatment of the electron collisional heating of the neutral gas. When hydrodynamic flow and the adiabatic cooling effect are included, atmospheric blowoff is prevented, and the Earth's exobase temperatures decrease with increasing solar EUV flux beyond a critical solar EUV flux. The transition from the hydrostatic equilibrium regime to the hydrodynamic flow regime occurs when the exobase temperature reaches 7000 to 8000 K if atomic O and N dominate the upper thermosphere. All of this implies that hydrodynamic flow and the associated adiabatic cooling

cannot be ignored when studying the early thermospheres of the Earth.

[50] 2. The fast variation of the bulk motion velocities under different exobase temperatures suggests that the adiabatic cooling effect could have kept the exobase temperature lower than ~1000 K if light gases such as atomic hydrogen were the dominant species in the Earth's thermosphere. We propose that hydrodynamic flow and associated adiabatic cooling should be important in the thermospheres of a broad range of terrestrial planets (early and/or close-in) and that the adiabatic cooling effect (acting as a thermostat) must be included in the energy equation in order to estimate their thermospheric structures and evolutionary paths correctly.

[51] **Acknowledgments.** We thank Christopher Smithtro and another anonymous reviewer for their helpful comments and suggestions, which helped to improve this manuscript. We thank Y. Deng, J. H. Lei, L. Y. Qian, S. C. Solomon, and W. B. Wang for helpful discussions. F. Tian thanks the High Altitude Observatory of NCAR for providing the computing facilities. F. Tian was partially supported by NASA Planetary Atmospheres grant NNGO5GA53G. H.-L. Liu and R. G. Roble's efforts are in part supported by the Office of Naval Research (N00014–07-C0209). This work was performed as part of the NASA Astrobiology Institute's Virtual Planetary Laboratory Lead Team, supported by the NASA through the NASA Astrobiology Institute under Cooperative Agreement CAN-00-OSS-01. This research was supported by the NASA Postdoctoral Program, administered by Oak Ridge Associated Universities through a contract with NASA.

References

Avakyan, S. V., et al. (1998), *Collision Processes and Excitation of UV Emission From Planetary Atmospheric Gases*, Gordon and Breach, Amsterdam, Netherland.

Banks, P. M., and G. Kockarts (1973), *Aeronomy*, Academic, New York.

Barth, C. A., A. I. F. Stewart, S. W. Bougher, D. M. Hunten, S. J. Bauer, and A. F. Nagy (1992), Aeronomy of the current Martian atmosphere, in *Mars, Space Science Series*, edited by H. H. Kieffer et al., pp. 1054–1089, Univ. of Ariz. Press, Tucson.

Bilitza, D. (1991), Solar-terrestrial models at the National Space Science Data Center, *J. Atmos. Terr. Phys.*, *53*, 1207–1211, doi:10.1016/0021-9169(91)90072-F.

Bilitza, D. (2001), International Reference Ionosphere 2000, *Radio Sci.*, *36*(2), 261–275, doi:10.1029/2000RS002432.

Bougher, S. W., S. Engel, R. G. Roble, and B. Foster (1999), Comparative terrestrial planet thermospheres: 2. Solar cycle variation of global structure and winds at equinox, *J. Geophys. Res.*, *104*, 16,591–16,611, doi:10.1029/1998JE001019.

Bougher, S. W., R. G. Roble, and T. Fuller-Rowell (2002), Simulations of the upper atmospheres of the terrestrial planets, in *Atmospheres in the Solar System: Comparative Aeronomy*, *Geophys. Monogr. Ser.*, vol. 130, edited by M. Mendillo, A. Nagy, and J. H. Waite, pp. 261–288, AGU, Washington, D. C.

Brinton, H. C., M. W. Pharo III, H. G. Mayr, and H. A. Taylor Jr. (1969), Implications for ionospheric chemistry and dynamics of a direct measurement of ion composition in the F_2 region, *J. Geophys. Res.*, *74*, 2941–2951, doi:10.1029/JA074i011p02941.

Chamberlain, J. W., and D. M. Hunten (1987), *Theory of Planetary Atmospheres*, Academic, Orlando, Fla.

Chassefière, E. (1996), Hydrodynamic escape of hydrogen from a hot water-rich atmosphere: The case of Venus, *J. Geophys. Res.*, *101*, 26,039–26,056, doi:10.1029/96JE01951.

Donahue, T. M. (1968), Ionospheric composition and reactions, *Science*, *159*, 489–498, doi:10.1126/science.159.3814.489.

Fennelly, J. A., and D. G. Torr (1992), Photoionization and photoabsorption cross sections of O, N_2, O_2, and N for aeronomic calculations, *At. Data Nucl. Data Tables*, *51*, 321, doi:10.1016/0092-640X(92)90004-2.

Fomichev, V. I., J. P. Blanchet, and D. S. Turner (1998), Matrix parameterization of the 15 μm CO_2 band cooling in the middle and upper atmosphere for variable CO_2 concentration, *J. Geophys. Res.*, *103*, 11,505–11,528, doi:10.1029/98JD00799.

Fox, J. L., and A. Dalgarno (1979), Ionization, luminosity, and heating of the upper atmosphere of Mars, *J. Geophys. Res.*, *84*, 7315–7333, doi:10.1029/JA084iA12p07315.

García-Muñoz, A. (2007), Physical and chemical aeronomy of HD 209458b, *Planet. Space Sci.*, *55*(10), 1426–1455, doi:10.1016/j.pss.2007.03.007.

Gordiets, B. F., Y. N. Kulikov, M. N. Markov, and M. Y. Marov (1982), Numerical modeling of the thermospheric heat budget, *J. Geophys. Res.*, *87*, 4504–4514, doi:10.1029/JA087iA06p04504.

Hedin, A. E. (1991), Extension of the MSIS thermosphere model into the middle and lower atmosphere, *J. Geophys. Res.*, *96*, 1159–1172, doi:10.1029/90JA02125.

Hoffman, J. H., C. Y. Johnson, J. C. Holmes, and J. M. Young (1969), Daytime midlatitude ion composition measurements, *J. Geophys. Res.*, *74*, 6281–6290, doi:10.1029/JA074i026p06281.

Hunten, D. M., and D. F. Strobel (1974), Production and escape of terrestrial hydrogen, *J. Atmos. Sci.*, *31*, 305–317, doi:10.1175/1520-0469(1974)031<0305:PAEOTH>2.0.CO;2.

Jeans, J. H. (1925), *The Dynamical Theory of Gases*, Cambridge Univ. Press, London.

Jet Propulsion Laboratory (1994), Chemical kinetics and photochemical data for use in stratospheric modeling, *JPL Publ.*, *94-26*, 15 Dec.

Kasting, J. F., and J. B. Pollack (1983), Loss of water from Venus. I. Hydrodynamic escape of hydrogen, *Icarus*, *53*, 479–508, doi:10.1016/0019-1035(83)90212-9.

Krasnopolsky, V. A. (1999), Hydrodynamic escape of N2 from Pluto, *J. Geophys. Res.*, *104*, 5955–5962, doi:10.1029/1998JE900052.

Kulikov, Y. N., et al. (2006), Atmospheric and water loss from early Venus, *Planet. Space Sci.*, *54*, 1425–1444, doi:10.1016/j.pss.2006.04.021.

Kulikov, Y. N., H. Lammer, H. Lichtenegger, T. Penz, D. Breuer, T. Spohn, R. Lundin, and H. K. Biernat (2007), A comparative study of the influence of the active young Sun on the early atmospheres of Earth, Venus, and Mars, *Space Sci. Rev.*, *129*, 207–243, doi:10.1007/s11214-007-9192-4.

Kumar, S., D. M. Hunten, and J. B. Pollack (1983), Nonthermal escape of hydrogen and deuterium from Venus and implications for loss of water, *Icarus*, *55*, 369–389, doi:10.1016/0019-1035(83)90109-4.

Lammer, H., F. Selsis, I. Ribas, E. F. Guinan, S. J. Bauer, and W. W. Weiss (2003), Atmospheric loss of exoplanets resulting from stellar X-ray and extreme-ultraviolet heating, *Astrophys. J. Lett.*, *598*, L121–L124, doi:10.1086/380815.

Lammer, H., et al. (2007), CME activity of low mass M stars as an important factor for the habitability of terrestrial exoplanets, part II: CME induced ion pick up of Earth-like exoplanets in close-in habitable zones, *Astrobiology*, *7*, 185–207, doi:10.1089/ast.2006.0128.

Nagy, A. F., T. E. Cravens, and T. I. Gombosi (1983), Basic theory and model calculations of the Venus ionosphere, in *Venus, Space Science Series*, edited by D. M. Hunten et al., pp. 841–872, Univ. of Ariz. Press, Tucson.

Öpik, E. J. (1963), Selective escape of gases, *Geophys. J.R. Astron. Soc.*, *7*, 490–526.

Parker, E. N. (1963), *Interplanetary Dynamical Processes*, Wiley-Interscience, New York.

Rees, M. H. (1989), *Physics and Chemistry of the Upper Atmosphere*, Cambridge Univ. Press, New York.

Ribas, I., E. F. Guinan, M. Güdel, and M. Audard (2005), Evolution of the solar activity over time and effects on planetary atmospheres. I. High-energy irradiances (1–1700 A), *Astrophys. J.*, *622*, 680–694, doi:10.1086/427977.

Richards, P. G., J. A. Fennelly, and D. G. Torr (1994), EUVAC: A solar EUV flux model for aeronomic calculations, *J. Geophys. Res.*, *99*, 8981–8992, doi:10.1029/94JA00518.

Roble, R. G. (1995), Energetics of the mesosphere and thermosphere, in *The Upper Mesosphere and Lower Thermosphere: A Review of Experiment and Theory*, *Geophys. Monogr. Ser*, vol. 87, edited by R. M. Johnson and T. L. Killeen, pp. 1–21, AGU, Washington, D. C.

Roble, R. G., E. C. Rodley, and R. E. Dickinson (1987), On the global mean structure of the thermosphere, *J. Geophys. Res.*, *92*, 8745–8758, doi:10.1029/JA092iA08p08745.

Rottman, G. J., et al. (1986), *Atmospheric ozone, assessment of our understanding of processes controlling its present distribution and change*, *Rep. 16*, vol. 1, World Meteorol. Org., Global Ozone Res. and Monit. Proj., Washington, D. C.

Schunk, R. W., and A. F. Nagy (2000), *Ionospheres: Physics, Plasma Physics, and Chemistry*, Cambridge Univ. Press, New York.

Smithtro, C. G., and J. J. Sojka (2005a), A new global average model of the coupled thermosphere and ionosphere, *J. Geophys. Res.*, *110*, A08305, doi:10.1029/2004JA010781.

Smithtro, C. G., and J. J. Sojka (2005b), Behavior of the ionosphere and thermosphere subject to extreme solar cycle conditions, *J. Geophys. Res.*, *110*, A08306, doi:10.1029/2004JA010782.

Solomon, S. C., and L. Qian (2005), Solar extreme-ultraviolet irradiance for general circulation models, *J. Geophys. Res.*, *110*, A10306, doi:10.1029/2005JA011160.

Strobel, D. F. (2007), Titan's hydrodynamically escaping atmosphere, *Icarus*, *193*(2), 588–594, doi:10.1016/j.icarus.2007.08.014.

Strobel, D. F. (2008), N2 escape rates from Pluto's atmosphere, *Icarus*, *193*, 612.

Tian, F., and O. B. Toon (2005), Hydrodynamic escape of nitrogen from Pluto, *Geophys. Res. Lett.*, *32*, L18201, doi:10.1029/2005GL023510.

Tian, F., O. B. Toon, A. A. Pavlov, and H. DeSterck (2005a), Transonic hydrodynamic escape of hydrogen from extrasolar planetary atmospheres, *Astrophys. J.*, *621*, 1049–1060, doi:10.1086/427204.

Tian, F., O. B. Toon, A. A. Pavlov, and H. DeSterck (2005b), A hydrogen-rich early Earth atmosphere, *Science*, *308*, 1014–1017, doi:10.1126/science.1106983.

Walker, J. C. G. (1977), *Evolution of the Atmosphere*, Macmillan, New York.

Watson, A. J., T. M. Donahue, and J. C. G. Walker (1981), The dynamics of a rapidly escaping atmosphere: applications to the evolution of Earth and Venus, *Icarus*, *48*, 150–166, doi:10.1016/0019-1035(81)90101-9.

Woods, T. N., and G. J. Rottman (2002), Solar ultraviolet variability over time periods of aeronomic interest, in *Comparative Aeronomy in the Solar System*, *Geophys. Monogr. Ser*, vol. 130, edited by M. Mendillo, A. F. Nagy, and J. H. Waite, pp. 221–233, AGU, Washington, D. C.

Yan, M., H. R. Sadeghpour, and A. Dalgarno (1998), Photoionization cross sections of He and H_2, *Astrophys. J.*, *496*, 1044–1050, doi:10.1086/305420.

Yelle, R. V. (2004), Aeronomy of extrasolar giant planets at small orbital distances, *Icarus*, *170*, 167–179, doi:10.1016/j.icarus.2004.02.008. (Corrigendum to Aeronomy of extra-solar giant planets at small orbital distances, *Icarus*, *183*, 508, doi:10.1016/j.icarus.2006.05.001, 2006.)

Yung, Y. L., and W. B. DeMore (1999), *Photochemistry of Planetary Atmospheres*, Oxford Univ. Press, Oxford, U.K.

J. F. Kasting, Department of Geosciences, 443 Deike, Pennsylvania State University, University Park, PA 16802, USA.

H.-L. Liu, R. G. Roble, and F. Tian, High Altitude Observatory, National Center for Atmospheric Research, Boulder, CO 80307, USA. (tian@ucar.edu)